Journal of Computational Physics 230 (2011) 4353–4375

Contents lists available at ScienceDirect

Journal of Computational Physics

journal homepage: www.elsevier.com/locate/jcp

Local DG method using WENO type limiters for convection–diffusion problems

Jun Zhu [a], Jianxian Qiu [b,*]

[a] College of Science, Nanjing University of Aeronautics and Astronautics, Nanjing, Jiangsu 210016, PR China
[b] Department of Mathematics, Nanjing University, Nanjing, Jiangsu 210093, PR China

ARTICLE INFO

Article history:
Received 18 December 2009
Received in revised form 16 March 2010
Accepted 16 March 2010
Available online 21 March 2010

Keywords:
Weighted essentially non-oscillatory
Runge–Kutta time discretization
Discontinuous Galerkin method
Convection–diffusion equations
Limiters

ABSTRACT

The local discontinuous Galerkin (LDG) method is a spatial discretization procedure for convection–diffusion equations, which employs useful features from high resolution finite volume schemes, such as the exact or approximate Riemann solvers serving as numerical fluxes and limiters, which is termed as Runge–Kutta LDG (RKLDG) when TVD Runge–Kutta method is applied for time discretization. It has the advantage of flexibility in handling complicated geometry, *h-p* adaptivity, and efficiency of parallel implementation and has been used successfully in many applications. However, the limiters used to control spurious oscillations in the presence of strong shocks are less robust than the strategies of essentially non-oscillatory (ENO) and weighted ENO (WENO) finite volume and finite difference methods. In this paper, we investigated RKLDG methods with WENO and Hermite WENO (HWENO) limiters for solving convection–diffusion equations on unstructured meshes, with the goal of obtaining a robust and high order limiting procedure to simultaneously obtain uniform high order accuracy and sharp, non-oscillatory shock transition. Numerical results are provided to illustrate the behavior of these procedures.

1. Introduction

In this paper, we investigated the Runge–Kutta local discontinuous Galerkin (RKLDG) methods with weighted essentially non-oscillatory (WENO) and Hermite WENO (HWENO) limiters for solving convection–diffusion problems:

$$\begin{cases} \partial_t u + \nabla \cdot F_c(u) - \nabla \cdot F_d(u, \nabla u) = 0, \\ u(x, y, 0) = u_0(x, y), \end{cases} \tag{1.1}$$

on two dimensional unstructured meshes, with the goal of obtaining a robust and high order limiting procedure to simultaneously obtain uniform high order accuracy and sharp, non-oscillatory shock transition for the LDG methods.

In 1973, Reed and Hill [21] first introduced the discontinuous Galerkin (DG) method for solving neutron transport problem. From 1987, Cockburn and Shu developed the DG method in a series of papers [4–8], in which they established a framework to easily solve *nonlinear* time dependent hyperbolic conservation laws, using explicit, nonlinearly stable high order Runge–Kutta time discretizations [24] and DG discretization in space with exact or approximate Riemann solvers as interface fluxes and total variation bounded (TVB) limiter [23] to achieve nonoscillatory properties for strong shocks. These schemes are termed RKDG methods.

* Corresponding author. Tel.: +86 25 8359 6053; fax: +86 25 8359 7130.
E-mail addresses: zhujun@nuaa.edu.cn (J. Zhu), jxqiu@nju.edu.cn (J. Qiu).

0021-9991/$ - see front matter © 2010 Elsevier Inc. All rights reserved.
doi:10.1016/j.jcp.2010.03.023

An important component of RKDG methods for solving the conservation laws (1.1) with strong shocks in the solutions is a nonlinear limiter, which is applied to detect discontinuities and control spurious oscillations near such discontinuities. Many such limiters have been used in the literature on RKDG methods. For example, we mention the *minmod* type TVB limiter [4–8], which is a slope limiter using a technique borrowed from the finite volume methodology; the moment based limiter [2] and an improved moment limiter [3], which are specifically designed for discontinuous Galerkin methods and work on the moments of the numerical solution. These limiters tend to degrade accuracy when mistakenly used in smooth regions of the solution. In [19], Qiu and Shu investigated using weighted essentially nonoscillatory (WENO) finite volume methodology

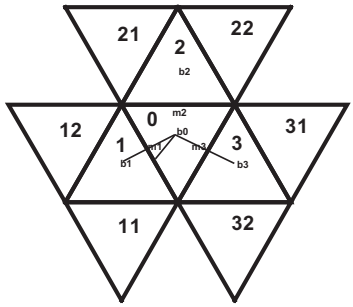

Fig. 1. The limiting diagram.

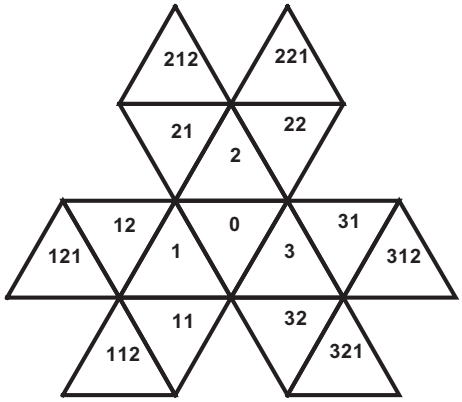

Fig. 2. The big stencil.

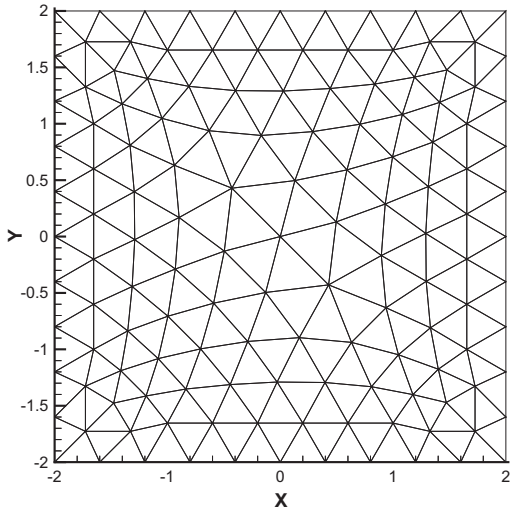

Fig. 3. Linear convection diffusion equation. Mesh. Triangle: $h = 4/10$.

[11,13–15] as limiter for RKDG method and in the papers [18,20] they presented Hermite weighted essentially non-oscillatory (HWENO) finite volume methodology as limiters for RKDG, for solving nonlinear hyperbolic conservation laws on structured meshes, with the goal of obtaining a robust and high order limiting procedure to simultaneously achieve uniform high order accuracy and sharp, nonoscillatory shock transition for the RKDG methods. The following framework has been adopted:

Table 1
$u_t + u_x + u_y = \frac{2a}{\pi^2}u_{xx} + \frac{2a}{\pi^2}u_{yy}$. $u(x,y,0) = \sin(0.5\pi(x+y))$. Periodic boundary conditions in both directions. $t = 1$, L^1 and L^∞ errors. RKLDG with the WENO limiter ($M = 0.01$) compared to RKLDG without limiter. The mesh points on the boundary are uniformly distributed with cell length h.

	h	RKLDG with WENO limiter				RKLDG without limiter			
		L^1 error	Order	L^∞ error	Order	L^1 error	Order	L^∞ error	Order
P^1	4/10	6.12E−2		2.19E−1		1.63E−2		7.81E−2	
	4/20	2.44E−2	1.33	9.38E−2	1.23	3.84E−3	2.09	2.24E−2	1.80
	4/40	6.14E−3	1.99	3.42E−2	1.46	9.15E−4	2.07	6.00E−3	1.90
	4/80	1.28E−3	2.26	1.07E−2	1.67	2.17E−4	2.07	1.52E−3	1.98
	4/160	2.38E−4	2.43	3.13E−3	1.78	5.13E−5	2.09	3.71E−4	2.03
P^2	4/10	7.05E−3		3.91E−2		6.91E−4		3.39E−3	
	4/20	1.34E−3	2.39	5.29E−3	2.88	8.20E−5	3.07	5.12E−4	2.72
	4/40	1.68E−4	2.99	7.90E−4	2.73	9.72E−6	3.07	6.55E−5	2.96
	4/80	1.58E−5	3.40	1.27E−4	2.63	1.09E−6	3.14	7.98E−6	3.03
	4/160	1.42E−6	3.47	1.77E−5	2.84	1.45E−7	2.91	9.31E−7	3.09

Table 2
$u_t + u_x + u_y = \frac{2a}{\pi^2}u_{xx} + \frac{2a}{\pi^2}u_{yy}$. $u(x,y,0) = \sin(0.5\pi(x+y))$. Periodic boundary conditions in both directions. $t = 1$, L^1 and L^∞ errors. RKLDG with the HWENO limiter ($M = 0.01$) compared to RKLDG without limiter. The mesh points on the boundary are uniformly distributed with cell length h.

	h	RKLDG with HWENO limiter				RKLDG without limiter			
		L^1 error	Order	L^∞ error	Order	L^1 error	Order	L^∞ error	Order
P^1	4/10	1.23E−1		3.59E−1		1.63E−2		7.81E−2	
	4/20	4.60E−2	1.42	1.68E−1	1.09	3.84E−3	2.09	2.24E−2	1.80
	4/40	1.59E−2	1.53	6.55E−2	1.37	9.15E−4	2.07	6.00E−3	1.90
	4/80	3.27E−3	2.28	2.20E−2	1.57	2.17E−4	2.07	1.52E−3	1.98
	4/160	5.83E−4	2.48	6.63E−3	1.73	5.13E−5	2.09	3.71E−4	2.03
P^2	4/10	6.97E−3		4.39E−2		6.91E−4		3.39E−3	
	4/20	1.00E−3	2.79	4.74E−3	3.21	8.20E−5	3.07	5.12E−4	2.72
	4/40	1.24E−4	3.02	5.50E−4	3.11	9.72E−6	3.07	6.55E−5	2.96
	4/80	1.38E−5	3.17	6.62E−5	3.05	1.09E−6	3.14	7.98E−6	3.03
	4/160	1.63E−6	3.08	9.68E−6	2.77	1.45E−7	2.91	9.31E−7	3.09

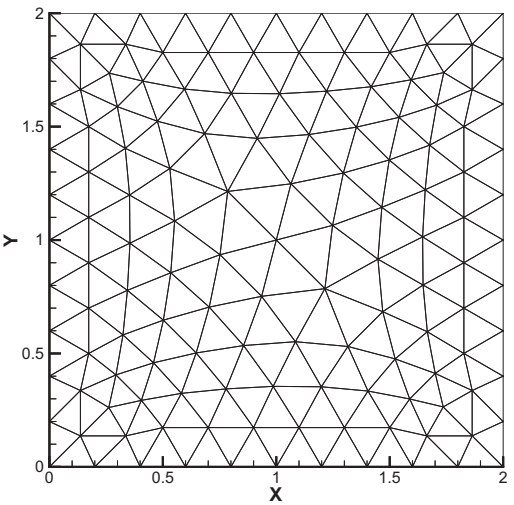

Fig. 4. 2D equations. Mesh. Triangle: $h = 2/10$.

Table 3
2D equations: initial data $\rho(x,y,0) = 1 + 0.2\sin(\pi(x+y))$, $u(x,y,0) = 0.5$, $v(x,y,0) = 0.5$, and $p(x,y,0) = 1$. Periodic boundary conditions in both directions. $t = 2$. Asymptotic convergence L^1 and L^∞ errors. RKLDG with the WENO limiter ($M = 0.01$) compared to RKLDG without limiter. The mesh points on the boundary are uniformly distributed with cell length h.

	h	RKLDG with WENO limiter				RKLDG without limiter			
		L^1 error	Order	L^∞ error	Order	L^1 error	Order	L^∞ error	Order
P^1	2/10	2.63E−2		5.69E−2		4.00E−3		1.67E−2	
	2/20	6.87E−3	1.94	1.66E−2	1.77	7.48E−4	2.42	3.81E−3	2.14
	2/40	1.42E−3	2.27	4.27E−3	1.96	1.65E−4	2.18	9.01E−4	2.08
	2/80	2.82E−4	2.33	1.15E−3	1.89	3.91E−5	2.08	2.17E−4	2.05
P^2	2/10	6.41E−3		2.04E−2		2.38E−4		9.37E−4	
	2/20	1.36E−3	2.24	4.32E−3	2.25	3.15E−5	2.92	1.85E−4	2.34
	2/40	1.73E−4	2.97	5.68E−4	2.93	4.12E−6	2.93	2.60E−5	2.83
	2/80	2.13E−5	3.02	7.62E−5	2.90	5.06E−7	3.02	3.07E−6	3.08

Table 4
2D equations: initial data $\rho(x,y,0) = 1 + 0.2\sin(\pi(x+y))$, $u(x,y,0) = 0.5$, $v(x,y,0) = 0.5$, and $p(x,y,0) = 1$. Periodic boundary conditions in both directions. $t = 2$. Asymptotic convergence L^1 and L^∞ errors. RKLDG with the HWENO limiter ($M = 0.01$) compared to RKLDG without limiter. The mesh points on the boundary are uniformly distributed with cell length h.

	h	RKLDG with HWENO limiter				RKLDG without limiter			
		L^1 error	Order	L^∞ error	Order	L^1 error	Order	L^∞ error	Order
P^1	2/10	3.05E−2		6.21E−2		4.00E−3		1.67E−2	
	2/20	9.24E−3	1.73	2.21E−2	1.49	7.48E−4	2.42	3.81E−3	2.14
	2/40	2.17E−3	2.09	7.18E−3	1.63	1.65E−4	2.18	9.01E−4	2.08
	2/80	4.53E−4	2.26	2.26E−3	1.67	3.91E−5	2.08	2.17E−4	2.05
P^2	2/10	4.69E−3		1.78E−2		2.38E−4		9.37E−4	
	2/20	9.52E−4	2.30	3.02E−3	2.56	3.15E−5	2.92	1.85E−4	2.34
	2/40	1.16E−4	3.03	3.79E−4	2.99	4.12E−6	2.93	2.60E−5	2.83
	2/80	1.38E−5	3.07	4.84E−5	2.97	5.06E−7	3.02	3.07E−6	3.08

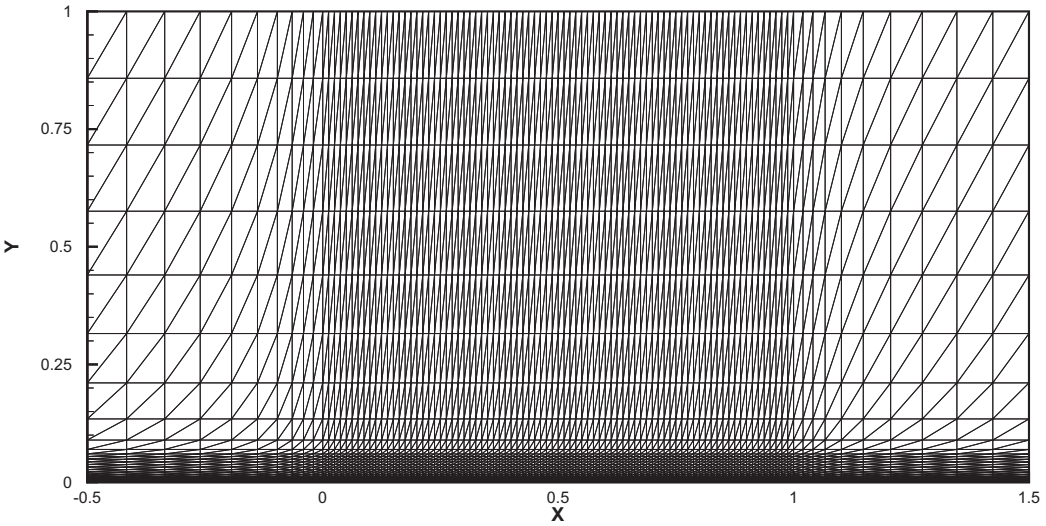

Fig. 5. The laminar flow problem. Mesh.

Table 5
The laminar flow problem. The maximum and average percentages of troubled cells subject to the WENO limiting.

	$M_\infty = 0.4$, $Re_\infty = 5000$ and $\alpha = 0^\circ$			
	M	1	50	100
P^1	Max. per	63.1	5.15	1.63
	Ave. per	49.2	0.97	0.40
P^2	Max. per	67.2	12.5	6.50
	Ave. per	55.2	9.65	0.87

Step 1: First, identify the "troubled cells", namely those cells which might need the limiting procedure.
Step 2: Then, replace the solution polynomials in those troubled cells by reconstructed algebraic polynomials using the WENO and HWENO methodologies which maintain the original cell averages, have the same orders of accuracy as before, but are less oscillatory.

Table 6
The laminar flow problem. The maximum and average percentages of troubled cells subject to the HWENO limiting.

	$M_\infty = 0.4,\ Re_\infty = 5000$ and $\alpha = 0^\circ$			
	M	1	50	100
P^1	Max. per	64.2	8.78	1.26
	Ave. per	47.7	0.70	0.12
P^2	Max. per	66.3	13.7	4.85
	Ave. per	61.1	8.88	0.97

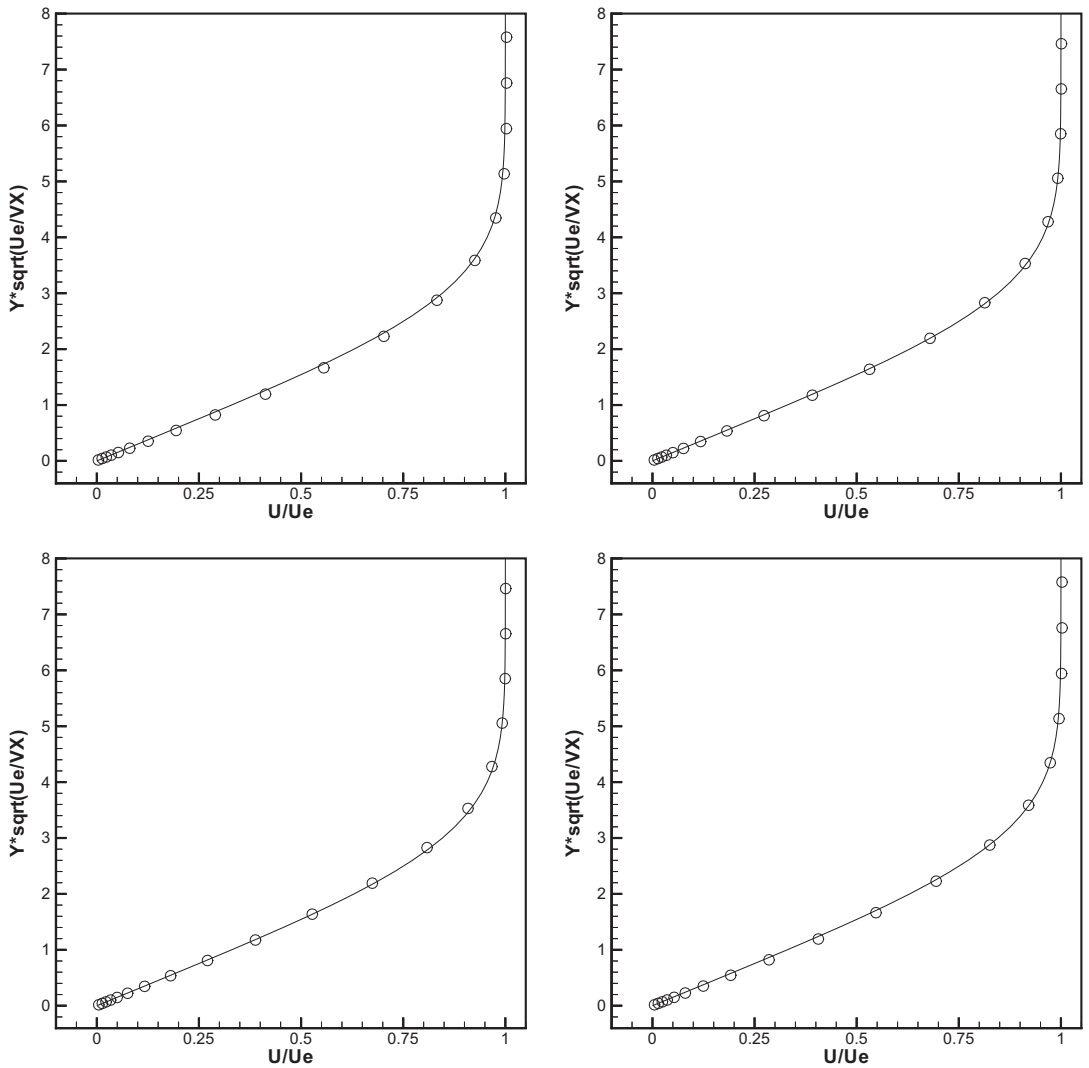

Fig. 6. The laminar flow problem. Velocity. Top: RKLDG with WENO limiter; bottom: RKLDG with HWENO limiter. Left: second order ($k = 1$); right: third order ($k = 2$). Solid line: reference solution; circles: the results of numerical schemes. The TVB constant $M = 100$.

This technique works quite well in one and two-dimensional test problems in [19] and in the followup work [18,20] where the more compact Hermite WENO methodology was used to reconstruct polynomials in the troubled cells on structured meshes. These methods were extended to unstructured meshes by Zhu et al. [26,27] and Luo et al. [17].

In 1997, Bassi and Rebay [1] extended a high order of discontinuous finite element method for the Euler equations to the case of the compressible Navier–Stokes equations without limiting procedure, providing the numerical solution is smooth enough. In [16], high order of accuracy was added by using spectral *hp* expansion on standard unstructured meshes by Lomtev and Karniadakis. It was more efficient and could get exponential accuracy and flow simulations on three dimensional unstructured meshes. In [9], Cockburn and Shu studied the local discontinuous Galerkin (LDG) methods for nonlinear time-dependent convection–diffusion systems. The proposed LDG methods are L^2-stable in the nonlinear case. An important part of DG methods for solving convection–diffusion equations (1.1) is the treatment of diffusion term. The treatment in [9] is to suitably rewrite the convection–diffusion system into a larger, degenerate, first-order system and then discretize it by the RKDG method. The other treatment was presented by Gassner et al. [12], they used the exact solution of the diffusive generalized Riemann problem to define a numerical flux discontinuous Galerkin schemes. The main advantage of this procedure is that the definition of the numerical flux is based on the same data as the advection flux, no different treatment of the diffusion terms is necessary, e.g. by assuming continuity at the grid cell interfaces.

In this continuation paper, we extend the method applied in [10,18–20,26,27] to solve convection–diffusion equations (1.1) on two dimensional unstructured meshes. We use the WENO and HWENO reconstructions based on the cell averages or derivative cell averages of neighboring cells to reconstruct the moments directly. This turns out to be a robust way to retain the original high order accuracy of the LDG method. The details of these procedures for the second and third order LDG methods with WENO and Hermite WENO limiters are described in Section 2 and the extensive numerical results are presented in Section 3 to verify the accuracy and stability of this approach. Concluding remarks are given in Section 4.

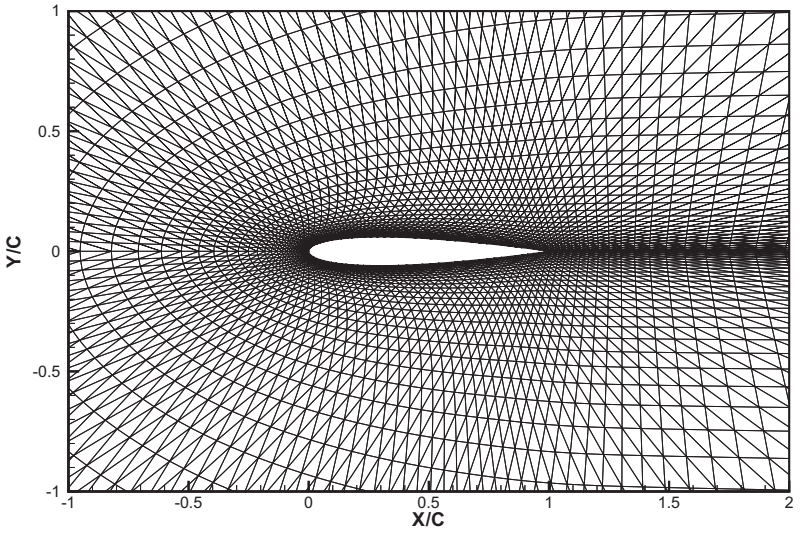

Fig. 7. NACA0012 airfoil mesh zoom in.

Table 7
NACA0012 airfoil problem. The maximum and average percentages of troubled cells subject to the WENO limiting and HWENO limiting. Case 1: $M_\infty = 0.8$, $Re_\infty = 73$ and $\alpha = 10^\circ$; case 2: $M_\infty = 2$, $Re_\infty = 106$ and $\alpha = 10^\circ$; case 3: $M_\infty = 0.85$, $Re_\infty = 2000$ and $\alpha = 0^\circ$; case 4: $M_\infty = 0.5$, $Re_\infty = 5000$ and $\alpha = 2^\circ$.

	M	Case 1			Case 2			Case 3			Case 4		
		1	10	100	1	10	100	1	10	100	1	10	100
RKLDG with WENO limiter													
P^1	Max. per	6.24	2.99	0.92	11.1	6.33	2.11	9.26	4.92	2.03	9.33	4.96	1.72
	Ave. per	3.63	1.56	0.43	8.96	5.61	1.85	4.64	1.32	0.25	3.80	1.19	0.27
P^2	Max. per	8.23	5.29	1.52	14.1	8.29	2.20	8.48	4.30	2.50	9.25	6.09	2.59
	Ave. per	3.53	2.01	0.53	8.75	5.49	1.28	3.37	1.14	0.18	2.61	1.50	0.16
RKLDG with HWENO limiter													
P^1	Max. per	7.78	3.28	0.97	13.8	6.88	2.27	11.1	5.24	1.90	10.0	4.53	1.55
	Ave. per	5.51	2.42	0.57	10.4	6.04	2.02	7.64	2.56	0.52	5.90	2.22	0.38
P^2	Max. per	9.01	4.98	1.52	14.8	8.82	2.49	9.40	4.70	2.09	9.33	5.03	1.93
	Ave. per	4.74	2.58	0.60	9.72	5.89	1.66	6.44	1.84	0.25	4.34	1.20	0.16

2. WENO and HWENO reconstructions as limiters to the RKLDG method on unstructured meshes

In this section we present the details of the procedures of RKLDG with WENO and HWENO limiters for solving convection–diffusion problems (1.1).

2.1. Description of RKLDG method

Given a triangulation consisting of cells Δ_j, $\mathbb{P}^k(\Delta_j)$ denotes the set of polynomials of degree at most k defined on Δ_j. Here k could actually change from cell to cell, but for simplicity we assume it is a constant over the whole triangulation. In the LDG method, the solution as well as the test function space is given by $V_h^k = \{v(x,y) : v(x,y)|_{\Delta_j} \in \mathbb{P}^k(\Delta_j)\}$. We emphasize that the procedure described below does not depend on the specific basis chosen for the polynomials. We adopt a local orthogonal basis over a target cell, such as $\Delta_0 : \{v_l^{(0)}(x,y),\ l = 0,\ldots,K; K = (k+1)(k+2)/2 - 1\}$:

$$
\begin{aligned}
v_0^{(0)}(x,y) &= 1,\\
v_1^{(0)}(x,y) &= \frac{x-x_0}{\sqrt{|\Delta_0|}},\\
v_2^{(0)}(x,y) &= a_{21}\frac{x-x_0}{\sqrt{|\Delta_0|}} + \frac{y-y_0}{\sqrt{|\Delta_0|}} + a_{22},\\
v_3^{(0)}(x,y) &= \frac{(x-x_0)^2}{|\Delta_0|} + a_{31}\frac{x-x_0}{\sqrt{|\Delta_0|}} + a_{32}\frac{y-y_0}{\sqrt{|\Delta_0|}} + a_{33},
\end{aligned}
$$

Table 8
NACA0012 airfoil problem. The lift, drag and moment of force coefficients subject to the WENO limiting and HWENO limiting. Case 1: $M_\infty = 0.8$, $Re_\infty = 73$ and $\alpha = 10^\circ$; case 2: $M_\infty = 2$, $Re_\infty = 106$ and $\alpha = 10^\circ$; case 3: $M_\infty = 0.85$, $Re_\infty = 2000$ and $\alpha = 0^\circ$; case 4: $M_\infty = 0.5$, $Re_\infty = 5000$ and $\alpha = 2^\circ$.

	M	Case 1			Case 2		
		1	10	100	1	10	100
RKLDG with WENO limiter							
P^1	*CL*	0.557	0.557	0.557	0.318	0.318	0.318
	CD	0.661	0.661	0.661	0.554	0.554	0.554
	CM	0.220	0.221	0.220	0.169	0.169	0.169
P^2	*CL*	0.582	0.582	0.582	0.305	0.305	0.305
	CD	0.664	0.664	0.664	0.570	0.570	0.571
	CM	0.226	0.226	0.227	0.163	0.162	0.163
		Case 3			Case 4		
P^1	*CL*	−3.69E−6	−3.62E−6	−3.65E−6	3.83E−2	3.83E−2	3.84E−2
	CD	0.116	0.116	0.116	5.27E−2	5.27E−2	5.27E−2
	CM	−1.41E−6	−1.33E−6	−1.33E−6	−6.73E−3	−6.73E−3	−6.73E−3
P^2	*CL*	1.09E−5	1.35E−5	1.05E−5	3.83E−2	3.83E−2	3.83E−2
	CD	0.120	0.120	0.120	5.60E−2	5.60E−2	5.60E−2
	CM	−9.26E−6	−7.92E−6	−8.94E−6	−6.42E−3	−6.41E−3	−6.42E−3
RKLDG with HWENO limiter							
		Case 1			Case 2		
P^1	*CL*	0.557	0.557	0.557	0.318	0.318	0.318
	CD	0.661	0.661	0.661	0.554	0.554	0.554
	CM	0.220	0.220	0.220	0.169	0.169	0.169
P^2	*CL*	0.581	0.581	0.582	0.303	0.303	0.303
	CD	0.663	0.663	0.663	0.566	0.566	0.566
	CM	0.226	0.226	0.226	0.161	0.161	0.161
		Case 3			Case 4		
P^1	*CL*	5.74E−5	6.03E−5	3.80E−5	3.85E−2	3.85E−2	3.85E−2
	CD	0.116	0.116	0.116	5.28E−2	5.28E−2	5.28E−2
	CM	5.40E−6	7.45E−6	3.93E−6	−6.70E−3	−6.69E−3	−6.70E−3
P^2	*CL*	1.31E−4	1.19E−4	1.02E−4	3.84E−2	3.83E−2	3.83E−2
	CD	0.120	0.120	0.120	5.60E−2	5.60E−2	5.60E−2
	CM	1.10E−5	1.34E−5	1.28E−5	−6.35E−3	−6.41E−3	−6.41E−3

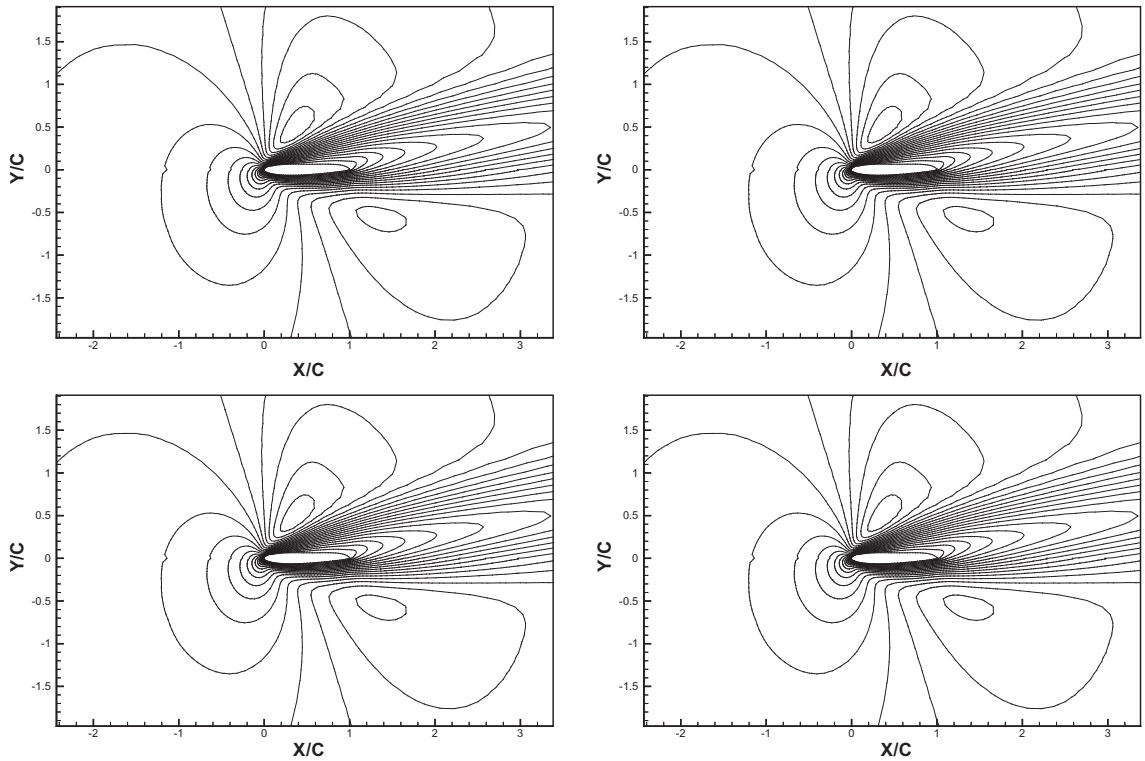

Fig. 8. NACA0012 airfoil. $M_\infty = 0.8$, $Re_\infty = 73$ and $\alpha = 10^\circ$. Mach number. Top: RKLDG with WENO limiter; bottom: RKLDG with HWENO limiter. Twenty equally spaced Mach number contours from 0.03 to 1.02. Left: $k = 1$; right: $k = 2$.

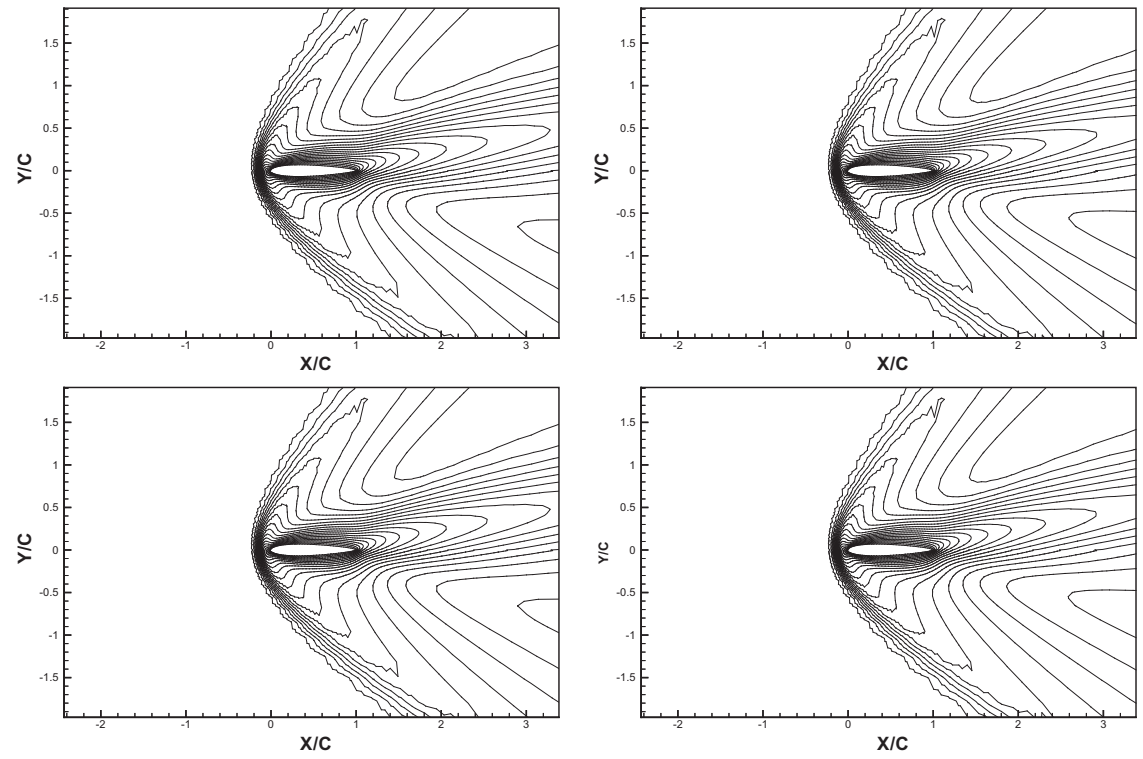

Fig. 9. NACA0012 airfoil. $M_\infty = 2$, $Re_\infty = 106$ and $\alpha = 10^\circ$. Mach number. Top: RKLDG with WENO limiter; bottom: RKLDG with HWENO limiter. Twenty equally spaced Mach number contours from 0.09 to 1.94. Left: $k = 1$; right: $k = 2$.

$$v_4^{(0)}(x,y) = a_{41}\frac{(x-x_0)^2}{|\Delta_0|} + \frac{(x-x_0)(y-y_0)}{|\Delta_0|} + a_{42}\frac{x-x_0}{\sqrt{|\Delta_0|}} + a_{43}\frac{y-y_0}{\sqrt{|\Delta_0|}} + a_{44},$$
$$v_5^{(0)}(x,y) = a_{51}\frac{(x-x_0)^2}{|\Delta_0|} + a_{52}\frac{(x-x_0)(y-y_0)}{|\Delta_0|} + \frac{(y-y_0)^2}{|\Delta_0|} + a_{53}\frac{x-x_0}{\sqrt{|\Delta_0|}} + a_{54}\frac{y-y_0}{\sqrt{\Delta_0}} + a_{55},$$
$$\ldots$$

where (x_0, y_0) and $|\Delta_0|$ are the barycenter and the area of the target cell Δ_0, respectively. Then we would need to solve a linear system to obtain the values of $a_{\ell m}$ by the orthogonality property:

$$\int_{\Delta_0} v_i^{(0)}(x,y)\, v_j^{(0)}(x,y)\,dx\,dy = w_i\delta_{ij} \tag{2.1}$$

with $w_i = \int_{\Delta_0}(v_i^{(0)}(x,y))^2\,dx\,dy$.

The numerical solution $u_h(x,y,t)$ in the space V_h^k can be written as:

$$u_h(x,y,t) = \sum_{l=0}^{K} u_0^{(l)}(t)\, v_l^{(0)}(x,y), \quad \text{for } (x,y) \in \Delta_0$$

and the degrees of freedom $u_0^{(l)}(t)$ are the moments defined by:

$$u_0^{(l)}(t) = \frac{1}{w_l}\int_{\Delta_0} u_h(x,y,t)\, v_l^{(0)}(x,y)\,dx\,dy, \quad l = 0,\ldots,K.$$

We use the methodology that adopted in [1,9,16]: let the gradient of the conservative variables $\nabla u = q(u)$ to be the auxiliary unknowns of the convection–diffusion equation, and Eq. (1.1) is reformulated as the coupled system for the unknowns q and u:

$$\begin{cases} q - \nabla u = 0, \\ \partial_t u + \nabla\cdot F_c(u) - \nabla\cdot F_d(u,q) = 0. \end{cases} \tag{2.2}$$

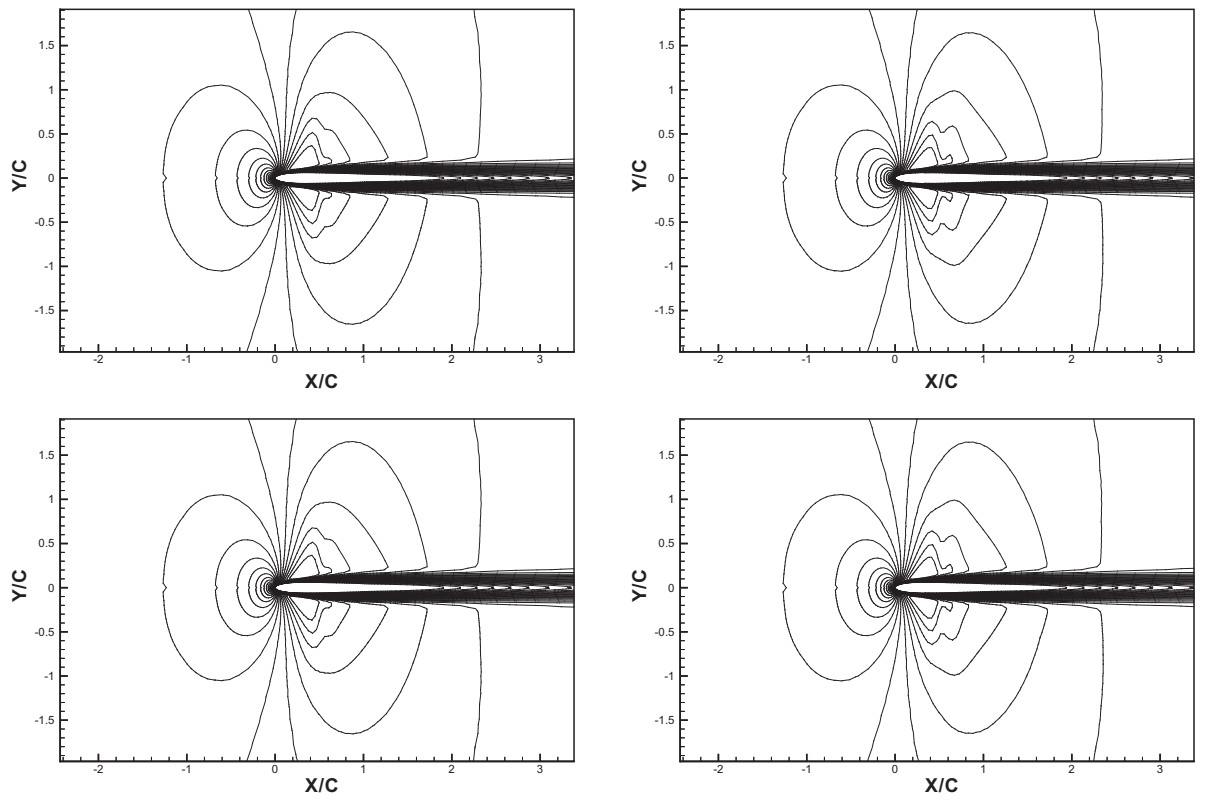

Fig. 10. NACA0012 airfoil. $M_\infty = 0.85$, $Re_\infty = 2000$ and $\alpha = 0^\circ$. Mach number. Top: RKLDG with WENO limiter; bottom: RKLDG with HWENO limiter. Thirty equally spaced Mach number contours from 0.05 to 1.05. Left: $k = 1$; right: $k = 2$.

Reconstruction of $q_h = \sum_{l=0}^{K} q_0^{(l)} v_l^{(0)}(x,y)$ to approximate to $q = \nabla u$ in Δ_0 in V_h^k. Multiply q with a basis $v_0^{(l)}(x,y),\ l = 0,1,\ldots,K$ of V_h^k, and integrate the first equation of (2.2) over the cell Δ_0, we obtain:

$$q_0^{(l)} = \frac{1}{w_l}\left(-\int_{\partial\Delta_0} v_l^{(0)}(x,y)u_h(x,y,t)\cdot n\,ds + \int_{\Delta_0} u_h(x,y,t)\cdot\nabla v_l^{(0)}(x,y)dx\,dy\right), \tag{2.3}$$

where n is the outward unit normal of the triangle boundary $\partial\Delta_0$. In (2.3) the volume integral terms can be computed exactly or by suitable numerical quadratures which are exact for polynomials of degree up to $2k$ for the element integral and up to $2k+1$ for the edge integral. In this paper, we use A_G Gaussian points ($A_G = 6$ for $k = 1$ and $A_G = 7$ for $k = 2$) for the element quadrature and E_G Gaussian points ($E_G = 2$ for $k = 1$ and $E_G = 3$ for $k = 2$) for the edge quadrature:

$$\int_{\Delta_0} u_h(x,y,t)\cdot\nabla v_l^{(0)}(x,y)dx\,dy \approx |\Delta_0|\sum_G \sigma_G u_h(x_G,y_G,t)\cdot\nabla v_l^{(0)}(x_G,y_G), \tag{2.4}$$

$$\int_{\partial\Delta_0} u_h(x,y,t)\,v_l^{(0)}(x,y)\cdot n\,ds \approx \sum_{ll=1}^{3}|\partial\Delta_{0_{ll}}|\sum_G \bar{\sigma}_G u_h(\bar{x}_{ll_G},\bar{y}_{ll_G},t))\,v_l^{(0)}(\bar{x}_{ll_G},\bar{y}_{ll_G})\cdot n_{ll}, \tag{2.5}$$

where $(x_G,y_G)\in\Delta_0$ and $(\bar{x}_{ll_G},\bar{y}_{ll_G})\in\partial\Delta_{0_{ll}}$ are the Gaussian quadrature points, and σ_G and $\bar{\sigma}_G$ are the Gaussian quadrature weights. Since the edge integral is on element boundaries where the numerical solution is discontinuous, we use a numerical flux function to replace $u_h(x,y,t)\cdot n$. Since we are constructing the discrete analogue of a diffusive operator, we define the numerical flux function as: $u_h^+\cdot n$, where u^+ are the values of u_h outside the cell Δ_0 (inside the neighboring cell) at the Gaussian point $(\bar{x}_{ll_G},\bar{y}_{ll_G},t)$. The test function $v_l^{(0)}$ in the boundary integral in (2.5) is taken from inside the cell Δ_0. The computed auxiliary variables $q_h(x,y)$ are then used in the weak form of the second equation of (2.2).

In order to determine the approximate solution, we evolve the degrees of freedom $u_0^{(l)}(t)$:

$$\begin{aligned}\frac{d}{dt}u_0^{(l)}(t) = \frac{1}{w_l}\Bigg(&\int_{\Delta_0}(F_c(u_h(x,y,t)) - F_d(u_h(x,y,t),q_h(x,y)))\cdot(\nabla v_l^{(0)}(x,y))dx\,dy\\ &-\int_{\partial\Delta_0}(F_c(u_h(x,y,t)) - F_d(u_h(x,y,t),q_h(x,y)))\cdot n\,v_l^{(0)}(x,y)ds\Bigg),\quad l = 0,\ldots,K.\end{aligned} \tag{2.6}$$

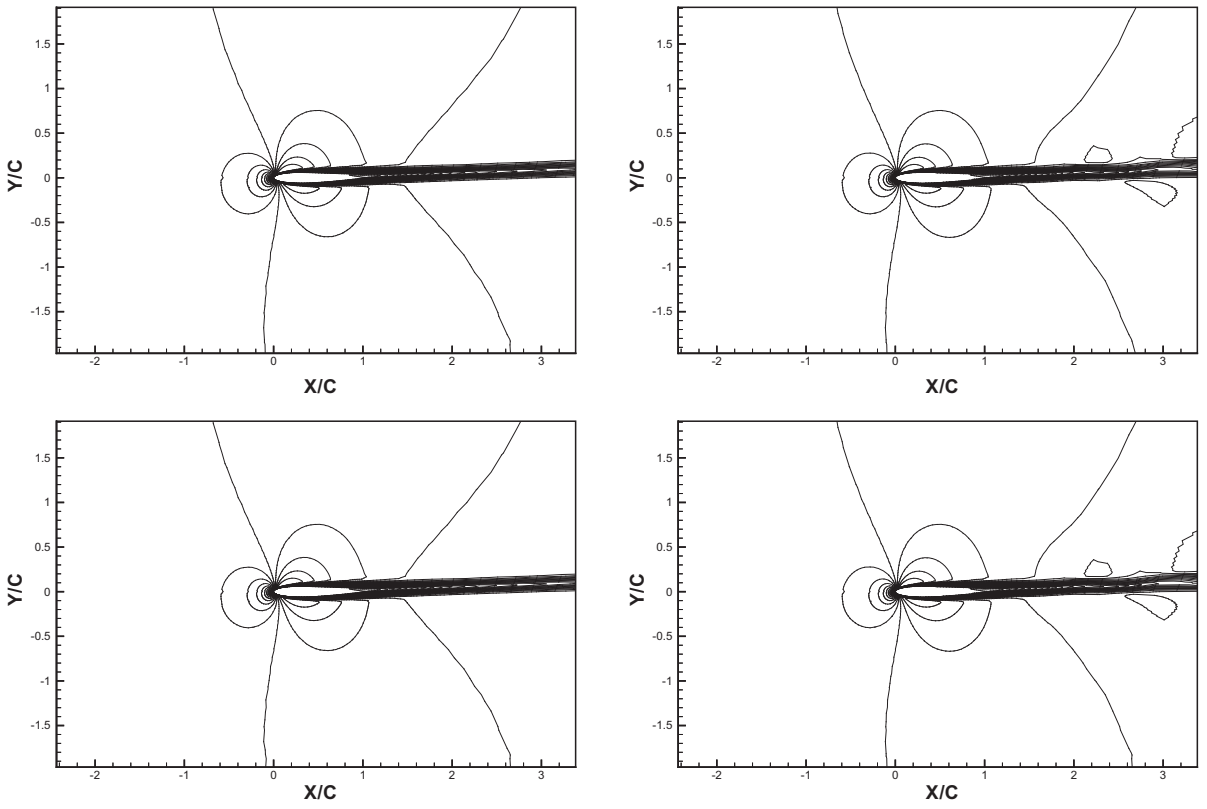

Fig. 11. NACA0012 airfoil. $M_\infty = 0.5, Re_\infty = 5000$ and $\alpha = 2^\circ$. Mach number. Top: RKLDG with WENO limiter; bottom: RKLDG with HWENO limiter. Thirty equally spaced Mach number contours from 0.01 to 0.58. Left: $k = 1$; right: $k = 2$.

In (2.6) the volume integral terms again can be computed either exactly or by suitable numerical quadratures which are exact for polynomials of degree up to $2k$ for the element integral and up to $2k+1$ for the edge integral. We use:

$$\int_{\Delta_0} (F_c(u_h(x,y,t)) - F_d(u_h(x,y,t), q_h(x,y))) \cdot (\nabla v_l^{(0)}(x,y)) dx\,dy \approx |\Delta_0| \sum_G \sigma_G (F_c(u_h(x_G,y_G,t)) - F_d(u_h(x_G,y_G,t), q_h(x_G,y_G))) \cdot (\nabla v_l^{(0)}(x_G,y_G)), \tag{2.7}$$

$$\int_{\partial\Delta_0} (F_c(u_h(x,y,t)) - F_d(u_h(x,y,t), q_h(x,y))) \cdot n v_l^{(0)}(x,y) ds \approx \sum_{ll=1}^{3} |\partial\Delta_{0_{ll}}| \sum_G \bar{\sigma}_G (F_c(u_h(\bar{x}_{ll_G}, \bar{y}_{ll_G}, t)) - F_d(u_h(\bar{x}_{ll_G}, \bar{y}_{ll_G}, t), q_h(\bar{x}_{ll_G}, \bar{y}_{ll_G}))) \cdot n_{ll} v_l^{(0)}(\bar{x}_{ll_G}, \bar{y}_{ll_G}), \tag{2.8}$$

where $(x_G, y_G) \in \Delta_0$ and $(\bar{x}_{ll_G}, \bar{y}_{ll_G}) \in \partial\Delta_{0_{ll}}$ are the Gaussian quadrature points, and σ_G and $\bar{\sigma}_G$ are the Gaussian quadrature weights. Since the edge integral is on element boundaries where the numerical solution is discontinuous, the flux of convection term $F_c(u_h(x,y,t)) \cdot n$ at Gaussian quadrature point $(\bar{x}_{ll_G}, \bar{y}_{ll_G}, t)$ can be approximated by a monotone numerical flux, such as the simple Lax–Friedrichs flux, which is given by:

$$F_c(u_h(\bar{x}_{ll_G}, \bar{y}_{ll_G}, t)) \cdot n \approx \frac{1}{2}\{(F_c(u^-(\bar{x}_{ll_G}, \bar{y}_{ll_G}, t)) + F_c(u^+(\bar{x}_{ll_G}, \bar{y}_{ll_G}, t))) \cdot n - \alpha(u^+(\bar{x}_{ll_G}, \bar{y}_{ll_G}, t) - u^-(\bar{x}_{ll_G}, \bar{y}_{ll_G}, t))\},$$

where α is taken as an upper bound for $|F_c'(u) \cdot n|$ in the scalar case, or the absolute value of eigenvalues of the Jacobian in the n direction for the system case, and u^- and u^+ are the values of u_h inside the cell Δ_0 and outside the cell Δ_0 (inside the neighboring cell) at the Gaussian point $(\bar{x}_{ll_G}, \bar{y}_{ll_G}, t)$. The idea of using such a numerical flux is borrowed from a finite volume methodology.

The flux of diffusion term $F_d(u_h(x,y,t), q_h(x,y)) \cdot n$ at Gaussian quadrature point $(\bar{x}_{ll_G}, \bar{y}_{ll_G}, t)$ can be approximated by numerical flux, such as:

$$F_d(u_h(\bar{x}_{ll_G}, \bar{y}_{ll_G}, t), q(\bar{x}_{ll_G}, \bar{y}_{ll_G})) \cdot n \approx F_d(u^-(\bar{x}_{ll_G}, \bar{y}_{ll_G}, t), q^-(\bar{x}_{ll_G}, \bar{y}_{ll_G})) \cdot n,$$

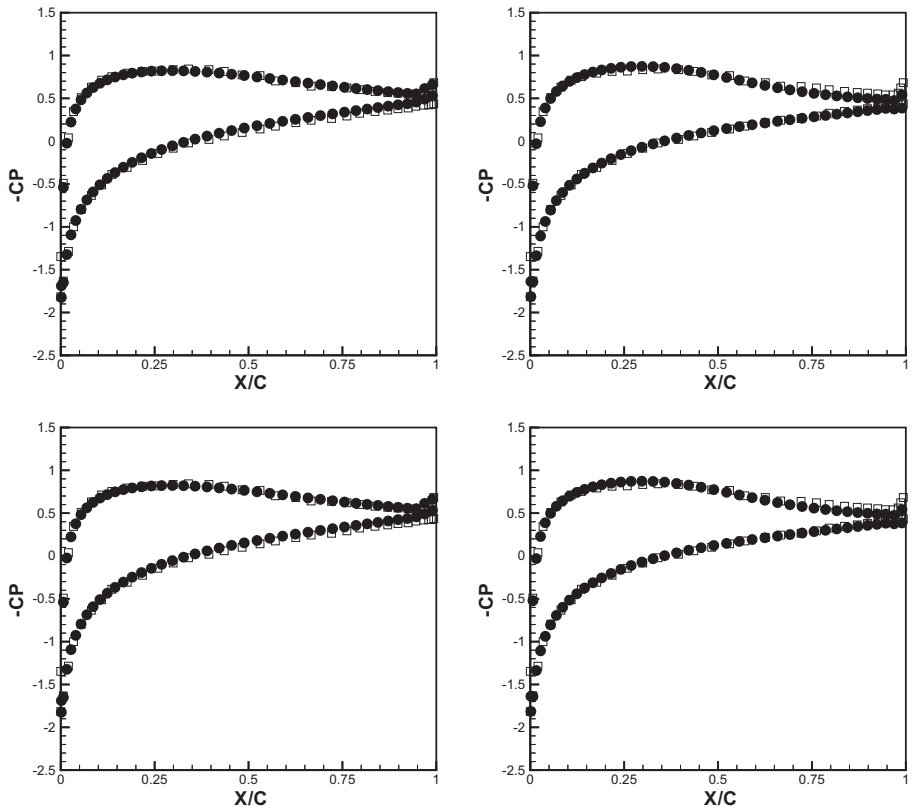

Fig. 12. NACA0012 airfoil. $M_\infty = 0.8$, $Re_\infty = 73$ and $\alpha = 10^\circ$. Pressure distribution. Top: RKLDG with WENO limiter; bottom: RKLDG with HWENO limiter. Left: $k = 1$; right: $k = 2$. Circles: numerical solution of RKLDG with (H) WENO limiters; squares: numerical solution of [1] ($k = 3$).

where q^- is the value of q_h inside the cell Δ_0 at the Gaussian point $(\bar{x}_{ll_G}, \bar{y}_{ll_G}, t)$. The test function $v_l^{(0)}(x,y)$ in the boundary integral in (2.8) is taken from inside the cell Δ_0.

The semi-discrete scheme (2.6) is discretized in time by a non-linear stable Runge–Kutta time discretization [24], e.g. the third-order version:

$$\begin{cases} u^{(1)} = u^n + \Delta t L(u^n), \\ u^{(2)} = \frac{3}{4}u^n + \frac{1}{4}u^{(1)} + \frac{1}{4}\Delta t L(u^{(1)}), \\ u^{n+1} = \frac{1}{3}u^n + \frac{2}{3}u^{(2)} + \frac{2}{3}\Delta t L(u^{(2)}). \end{cases} \tag{2.9}$$

The method described above can compute solutions to (1.1), which are either smooth or have weak shocks and other discontinuities, without further modification. If the discontinuities are strong, however, the scheme will generate significant oscillations and even nonlinear instability. To avoid such difficulties, we borrow the technique of a slope limiter from the finite volume methodology and use it after each Runge–Kutta inner stage (or after the complete Runge–Kutta time step) to control the numerical solution.

In this paper, we will use the limiter adopted in [8] only to detect "troubled cells". The main procedure is as follows. We use $(x_{m_\ell}, y_{m_\ell}),\ \ell = 1,2,3$, to denote the midpoints of the edges on the boundary of the target cell Δ_0, and $(x_{b_i}, y_{b_i}),\ i = 1,2,3$, to denote the barycenters of the neighboring triangles $\Delta_i,\ i = 1,2,3$, as shown in Fig. 1.

We then have:

$$x_{m_1} - x_{b_0} = \alpha_1(x_{b_1} - x_{b_0}) + \alpha_2(x_{b_3} - x_{b_0}), \quad y_{m_1} - y_{b_0} = \alpha_1(y_{b_1} - y_{b_0}) + \alpha_2(y_{b_3} - y_{b_0}) \tag{2.10}$$

with nonnegative $\alpha_1,\ \alpha_2$, which depend only on (x_{m_1}, y_{m_1}) and the geometry. We then define:

$$\tilde{u}_h(x_{m_1}, y_{m_1}, t) \equiv u_h(x_{m_1}, y_{m_1}, t) - u_0^{(0)}(t), \tag{2.11}$$

$$\Delta u(x_{m_1}, y_{m_1}, t) \equiv \alpha_1(u_1^{(0)}(t) - u_0^{(0)}(t)) + \alpha_2(u_3^{(0)}(t) - u_0^{(0)}(t)). \tag{2.12}$$

Using the TVB modified *minmod* function [23] defined as:

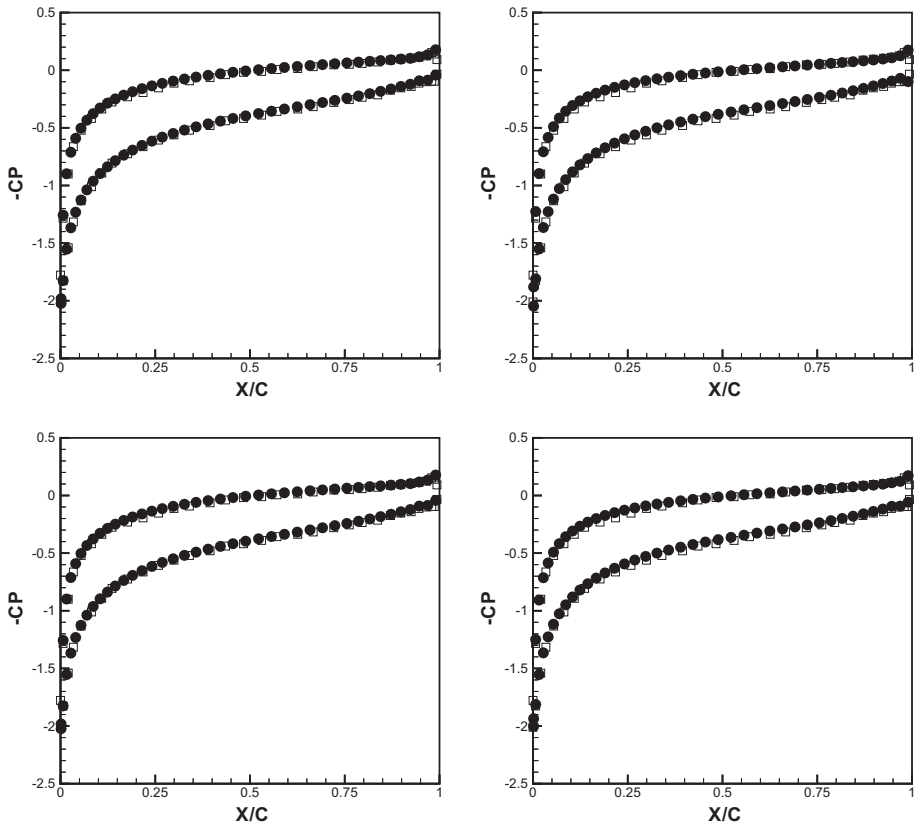

Fig. 13. NACA0012 airfoil. $M_\infty = 2,\ Re_\infty = 106$ and $\alpha = 10^\circ$. Pressure distribution. Top: RKLDG with WENO limiter; bottom: RKLDG with HWENO limiter. Left: second order $(k = 1)$; right: $k = 2$. Circles: numerical solution of RKLDG with (H) WENO limiters; squares: numerical solution of [1] $(k = 3)$.

$$\tilde{m}(a_1,a_2)=\begin{cases} a_1 & \text{if } |a_1|\leqslant M|\Delta_0|,\\ \begin{cases} s\min(|a_1|,|a_2|) & \text{if } s=sign(a_1)=sign(a_2)\\ 0 & \text{otherwise}\end{cases} & \text{otherwise},\end{cases} \tag{2.13}$$

where $M>0$ is the TVB constant whose choice is problem dependent, we can compute the quantity:

$$\tilde{u}^{mod}=\tilde{m}(\tilde{u}_h(x_{m_1},y_{m_1},t),\gamma\Delta u(x_{m_1},y_{m_1},t)) \tag{2.14}$$

with $\gamma>1$ (we take $\gamma=1.5$ in our numerical tests). If $\tilde{u}^{mod}\neq\tilde{u}_h(x_{m_1},y_{m_1},t)$, Δ_0 is marked as a "troubled cell" for further reconstruction. This procedure is repeated for the other two edges of Δ_0 as well. Since the WENO and HWENO reconstructions maintain high order accuracy in the troubled cells, it is less crucial to choose an accurate M. We present in Section 3 numerical tests obtained with different choices of M.

Remarks

(1) For the troubled cells, we reconstruct the algebraic polynomial solutions while retaining their cell averages. In other words, we reconstruct the degrees of freedom $u_0^{(l)}(t)$, $l=1,\ldots,K$ and retain only the cell average $u_0^{(0)}(t)$.
(2) For the WENO type reconstructions, when some triangles merge in the stencils, we can always use the next layer of triangles to overcome this drawback.

2.2. Description of WENO reconstruction as limiter for RKLDG

For the $k=1$ case, we summarize the procedure to reconstruct the first order moments $u_0^{(1)}(t)$ and $u_0^{(2)}(t)$ in the troubled cell Δ_0 using the WENO reconstruction procedure. For the simplicity, we rewrite $u_*^{(*)}(t)$ to be $u^{(*)}$ if it will not cause confusion. And we relabel the "troubled cell" and its neighboring cells shown in Fig. 2.

Step 2.1.1. We select the big stencil as $S=\{\Delta_0,\Delta_1,\Delta_2,\Delta_3,\Delta_{11},\Delta_{12},\Delta_{21},\Delta_{22},\Delta_{31},\Delta_{32}\}$. Then we construct polynomial $P(x,y)$ to approximate u by requiring that it has the same cell average as u on the target cell Δ_0, and matches the cell averages of u on the other triangles in the set $S\setminus\{\Delta_0\}$ in a least-square sense, see [13].

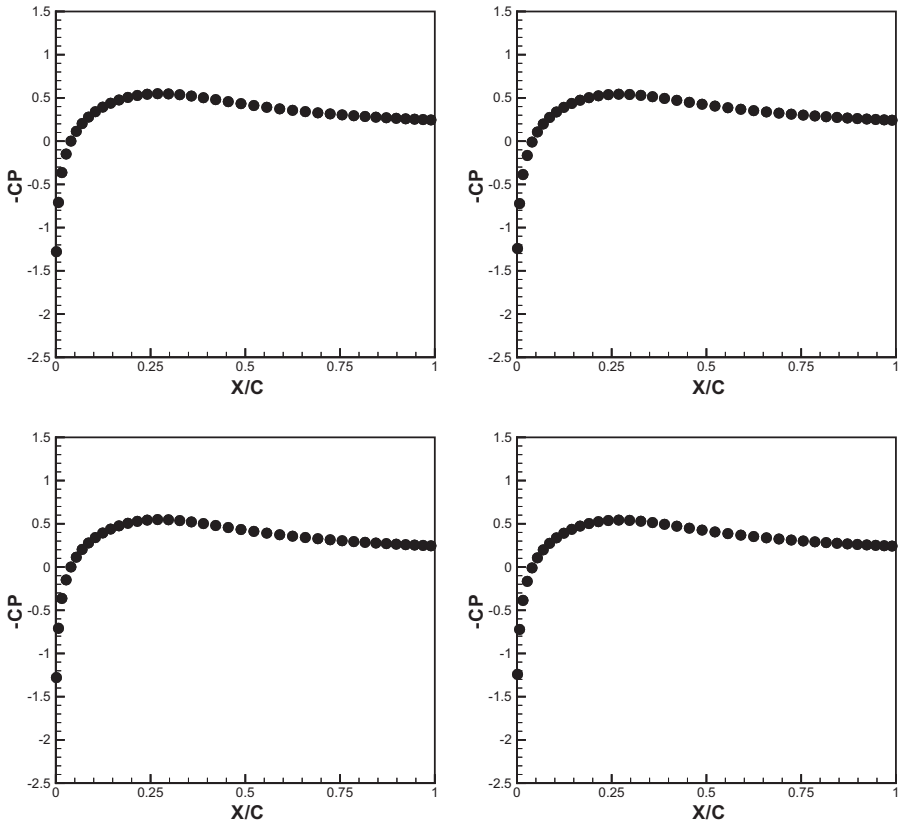

Fig. 14. NACA0012 airfoil. $M_\infty=0.85$, $Re_\infty=2000$ and $\alpha=0^\circ$. Pressure distribution. Top: RKLDG with WENO limiter; bottom: RKLDG with HWENO limiter. Left: $k=1$; right: $k=2$.

Step 2.1.2. We then construct nine linear polynomials $q_i(x,y),\ i=1,\ldots,9$, satisfying:

$$\frac{1}{|\Delta_\ell|}\int_{\Delta_\ell} q_i(x,y)dxdy = u_\ell^{(0)}. \tag{2.15}$$

For

$$\begin{aligned}
&i=1,\ \ell=0,1,2; \quad i=2,\ \ell=0,2,3; \quad i=3,\ \ell=0,3,1; \quad i=4,\ \ell=0,1,11;\\
&i=5,\ \ell=0,1,12; \quad i=6,\ \ell=0,2,21; \quad i=7,\ \ell=0,2,22; \quad i=8,\ \ell=0,3,31;\\
&i=9,\ \ell=0,3,32.
\end{aligned}$$

Step 2.1.3. We find the combination coefficients, also called linear weights, denoted by $\gamma_1^{(l)},\ldots,\gamma_9^{(l)},\ l=1,2$, satisfying:

$$\int_{\Delta_0} P(x,y)\,v_l^{(0)}(x,y)dxdy = \sum_{i=1}^{9}\gamma_i^{(l)}\int_{\Delta_0} q_i(x,y)\,v_l^{(0)}(x,y)dxdy, \quad l=1,2 \tag{2.16}$$

for the polynomial $P(x,y)$ defined before. The linear weights are achieved by asking for:

$$\min\left(\sum_{i=1}^{9}(\gamma_i^{(l)})^2\right), \quad l=1,2. \tag{2.17}$$

By doing so, we can get the linear weights uniquely but cannot guarantee the positiveness. We use the method introduced in [13,22] to overcome this difficulty.

Step 2.1.4. We compute the smoothness indicators, denote by $\beta_i,\ i=1,\ldots,9$, for the smaller stencils $S_i,\ i=1,\ldots,9$, which measure how smooth the functions $q_i(x,y),\ i=1,\ldots,9$ are in the target cell Δ_0. The smaller these smoothness indicators, the smoother the functions are in the target cell. We use the same recipe for the smoothness indicators as in [14]:

$$\beta_i = \sum_{|\ell|=1}^{k}|\Delta_0|^{|\ell|-1}\int_{\Delta_0}\left(\frac{\partial^{|\ell|}}{\partial x^{\ell_1}\partial y^{\ell_2}}q_i(x,y)\right)^2 dxdy, \tag{2.18}$$

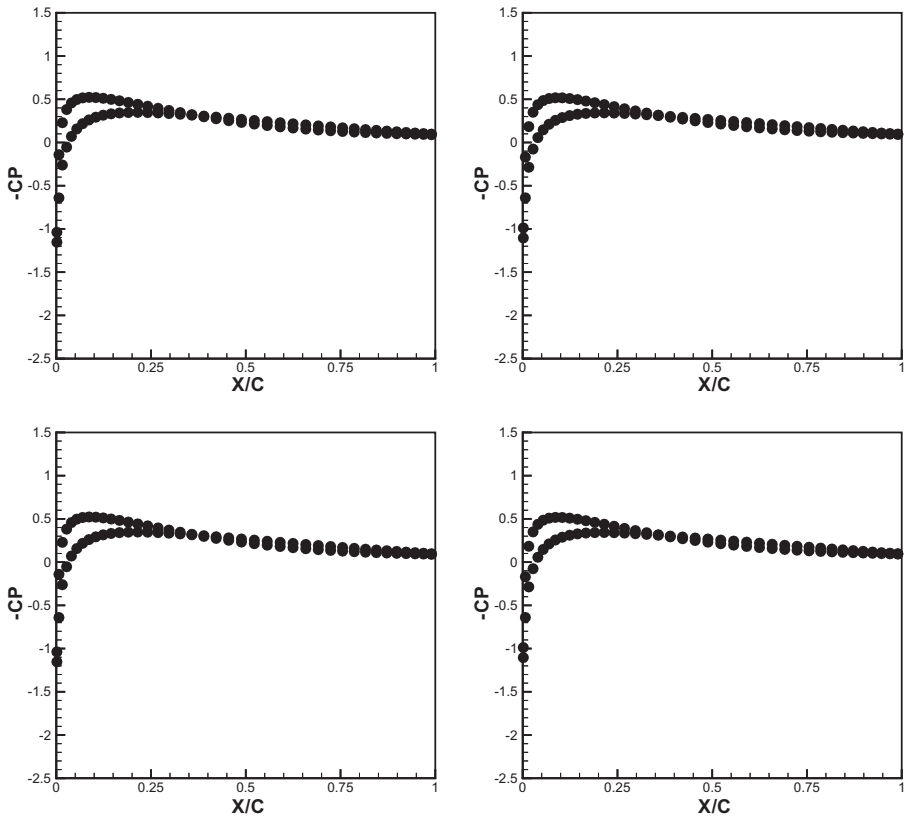

Fig. 15. NACA0012 airfoil. $M_\infty = 0.5,\ Re_\infty = 5000$ and $\alpha = 2^\circ$. Pressure distribution. Top: RKLDG with WENO limiter; bottom: RKLDG with HWENO limiter. Left: second order $(k=1)$; right: $k=2$.

where $\ell = (\ell_1, \ell_2)$.

Step 2.1.5. We compute the non-linear weights based on the smoothness indicators:

$$\omega_i^{(l)} = \frac{\bar{\omega}_i^{(l)}}{\sum_{\ell=1}^{9} \bar{\omega}_\ell^{(l)}}, \quad \bar{\omega}_\ell^{(l)} = \frac{\gamma_\ell^{(l)}}{(\varepsilon + \beta_\ell)^2}, \quad l = 1, 2. \tag{2.19}$$

Here ε is a small positive number to avoid the denominator to become zero. We take $\varepsilon = 10^{-3}$ in our computation.

The moments of the reconstructed polynomial are then given by:

$$u_0^{(l)}(t) = \frac{1}{\int_{\Delta_0} (v_l^{(0)}(x,y))^2 dx\,dy} \sum_{i=1}^{9} \omega_i^{(l)} \int_{\Delta_0} q_i(x,y)\, v_l^{(0)}(x,y) dx\,dy, \quad l = 1, 2. \tag{2.20}$$

For the $k = 2$ case, the procedure to reconstruct the first and second order moments $u_0^{(1)}$, $u_0^{(2)}$, $u_0^{(3)}$, $u_0^{(4)}$ and $u_0^{(5)}$ in the troubled cell Δ_0 is analogous to that for the $k = 1$ case. The troubled cell and its neighboring cells are shown in Fig. 2.

Step 2.2.1. We select the big stencil as $T = \{\Delta_0, \Delta_1, \Delta_2, \Delta_3, \Delta_{11}, \Delta_{12}, \Delta_{21}, \Delta_{22}, \Delta_{31}, \Delta_{32}, \Delta_{112}, \Delta_{121}, \Delta_{212}, \Delta_{221}, \Delta_{312}, \Delta_{321}\}$. Then we construct polynomial $Q(x,y)$ to approximate u by requiring that it has the same cell average as u on the target cell Δ_0 and matches the cell averages of u on the other triangles in the set $T \setminus \{\Delta_0\}$ in a least-square sense.

Step 2.2.2. We construct quadratic polynomials $q_i(x,y),\ i = 1, \ldots, 9$, which satisfy the following conditions:

$$\frac{1}{|\Delta_\ell|} \int_{\Delta_\ell} q_i(x,y) dx\,dy = u_\ell^{(0)}. \tag{2.21}$$

For

$$\begin{aligned}
&i = 1,\ \ell = 0, 1, 11, 12, 3, 32; \quad i = 2,\ \ell = 0, 1, 11, 12, 2, 21; \quad i = 3,\ \ell = 0, 2, 21, 22, 1, 12;\\
&i = 4,\ \ell = 0, 2, 21, 22, 3, 31; \quad i = 5,\ \ell = 0, 3, 31, 32, 2, 22; \quad i = 6,\ \ell = 0, 3, 31, 32, 1, 11;\\
&i = 7,\ \ell = 0, 1, 11, 12, 112, 121; \quad i = 8,\ \ell = 0, 2, 21, 22, 212, 221;\\
&i = 9,\ \ell = 0, 3, 31, 32, 312, 321.
\end{aligned}$$

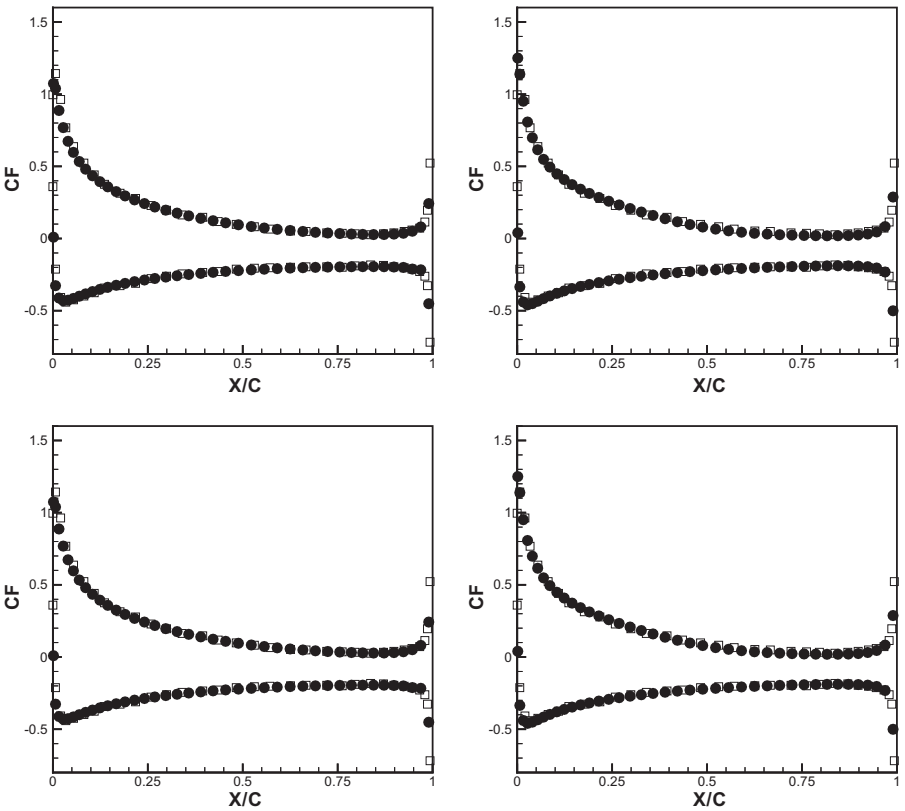

Fig. 16. NACA0012 airfoil. $M_\infty = 0.8$, $Re_\infty = 73$ and $\alpha = 10^\circ$. Skin friction coefficient distribution. Top: RKLDG with WENO limiter; bottom: RKLDG with HWENO limiter. Left: $k = 1$; right: $k = 2$. Circles: numerical solution of RKLDG with (H) WENO limiters; squares: numerical solution of [1] ($k = 3$).

The remaining steps 2.2.3, 2.2.4 and 2.2.5 are the same as those for the $k = 1$ case. Finally, the moments of the reconstructed polynomial are given by:

$$u_0^{(l)}(t) = \frac{1}{\int_{\Delta_0}(v_l^{(0)}(x,y))^2 dx\,dy} \sum_{i=1}^{9} \omega_i^{(l)} \int_{\Delta_0} q_i(x,y)\, v_l^{(0)}(x,y) dx\,dy, \quad l = 1,2,3,4,5. \tag{2.22}$$

2.3. Description of HWENO reconstruction as limiter for RKLDG

For the $k = 1$ case, we summarize the procedure to reconstruct the first order moments $u_0^{(1)}$ and $u_0^{(2)}$ in the troubled cell Δ_0 using the HWENO reconstruction procedure. The big stencil is shown in Fig. 2.

Step 2.3.1. We select the big stencil as $S = \{\Delta_0, \Delta_1, \Delta_2, \Delta_3\}$. Then we construct polynomial $P(x,y)$ to approximate u by requiring that it has the same cell average as $u^{(0)}$ on the target cell Δ_0, and matches the cell averages of $u^{(0)}$, $u^{(1)}$ or $u^{(2)}$ on the other triangles in the set $S \setminus \{\Delta_0\}$ in a least square sense.

Step 2.3.2. We then construct six linear polynomials $q_i(x,y)$, $i = 1, \ldots, 6$, satisfying:

$$\frac{1}{|\Delta_\ell|} \int_{\Delta_\ell} q_i(x,y) dx\,dy = u_\ell^{(0)}, \tag{2.23}$$

$$\frac{1}{\int_{\Delta_{\ell_x}}(v_1^{(\ell_x)}(x,y))^2 dx\,dy} \int_{\Delta_{\ell_x}} q_i(x,y)\, v_1^{(\ell_x)}(x,y) dx\,dy = u_{\ell_x}^{(1)}, \tag{2.24}$$

$$\frac{1}{\int_{\Delta_{\ell_y}}(v_2^{(\ell_y)}(x,y))^2 dx\,dy} \int_{\Delta_{\ell_y}} q_i(x,y)\, v_2^{(\ell_y)}(x,y) dx\,dy = u_{\ell_y}^{(2)}. \tag{2.25}$$

For

$$i = 1,\ \ell = 0,1,2; \quad i = 2,\ \ell = 0,2,3; \quad i = 3,\ \ell = 0,3,1; \quad i = 4,\ \ell = 0,\ \ell_x = 1,\ \ell_y = 1;$$
$$i = 5,\ \ell = 0,\ \ell_x = 2,\ \ell_y = 2; \quad i = 6,\ \ell = 0,\ \ell_x = 3,\ \ell_y = 3.$$

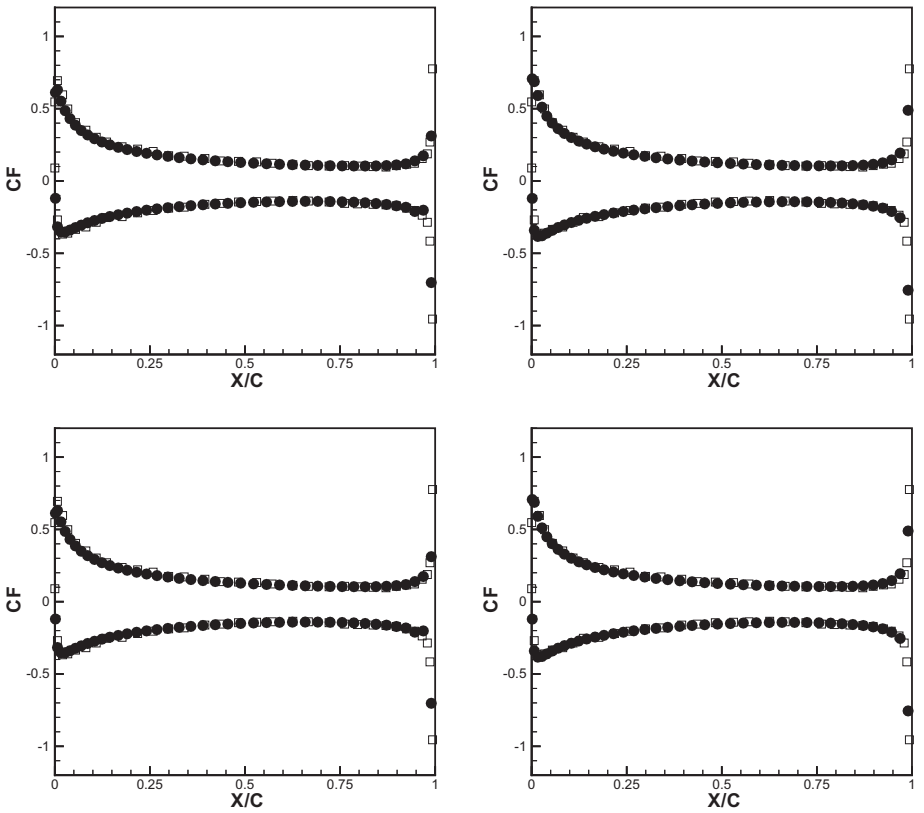

Fig. 17. NACA0012 airfoil. $M_\infty = 2$, $Re_\infty = 106$ and $\alpha = 10^\circ$. Skin friction coefficient distribution. Top: RKLDG with WENO limiter; bottom: RKLDG with HWENO limiter. Left: $k = 1$; right: $k = 2$. Circles: numerical solution of RKLDG with (H) WENO limiters; squares: numerical solution of [1] ($k = 3$).

Step 2.3.3. We find the combination coefficients, also called linear weights, denoted by $\gamma_1^{(l)},\ldots,\gamma_6^{(l)},\ l=1,2$, satisfying:

$$\int_{\Delta_0} P(x,y)v_l^{(0)}(x,y)dxdy=\sum_{i=1}^{6}\gamma_i^{(l)}\int_{\Delta_0} q_i(x,y)v_l^{(0)}(x,y)dxdy,\quad l=1,2. \tag{2.26}$$

The linear weights are achieved by asking for:

$$min\left(\sum_{i=1}^{6}(\gamma_i^{(l)})^2\right),\quad l=1,2. \tag{2.27}$$

Step 2.3.4. We compute the smoothness indicators, denote by $\beta_i,\ i=1,\ldots,6$, for the smaller stencils $S_i,\ i=1,\ldots,6$. We use the same recipe for the smoothness indicators as in [14]:

$$\beta_i=\sum_{|\ell|=1}^{k}|\Delta_0|^{|\ell|-1}\int_{\Delta_0}\left(\frac{\partial^{|\ell|}}{\partial x^{\ell_1}\partial y^{\ell_2}}q_i(x,y)\right)^2 dxdy, \tag{2.28}$$

where $\ell=(\ell_1,\ell_2)$.

Step 2.3.5. We compute the non-linear weights based on the smoothness indicators:

$$\omega_i^{(l)}=\frac{\bar{\omega}_i^{(l)}}{\sum_{\ell=1}^{6}\bar{\omega}_\ell^{(l)}},\quad \bar{\omega}_\ell^{(l)}=\frac{\gamma_\ell^{(l)}}{(\varepsilon+\beta_\ell)^2},\quad l=1,2. \tag{2.29}$$

The moments of the reconstructed polynomial are then given by:

$$u_0^{(l)}(t)=\frac{1}{\int_{\Delta_0}(v_l^{(0)}(x,y))^2dxdy}\sum_{i=1}^{6}\omega_i^{(l)}\int_{\Delta_0} q_i(x,y)v_l^{(0)}(x,y)dxdy,\quad l=1,2. \tag{2.30}$$

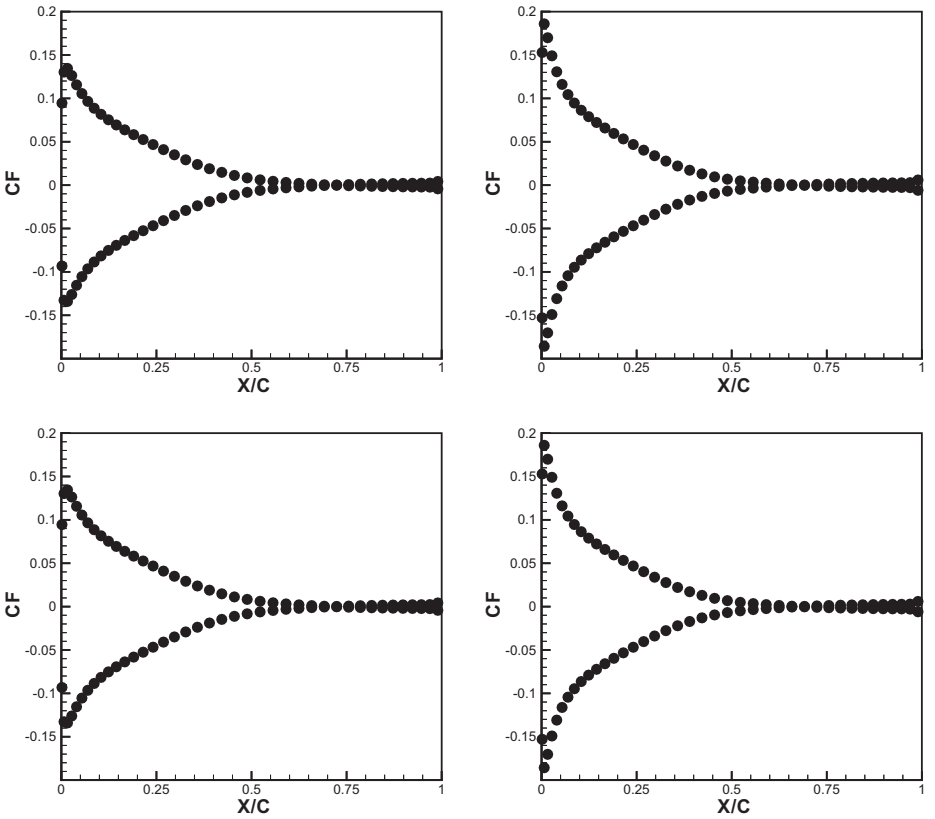

Fig. 18. NACA0012 airfoil. $M_\infty=0.85,\ Re_\infty=2000$ and $\alpha=0^\circ$. Skin friction coefficient distribution. Top: RKLDG with WENO limiter; bottom: RKLDG with HWENO limiter. Left: $k=1$; right: $k=2$.

For the $k=2$ case, the procedure to reconstruct the first and second order moments $u_0^{(1)}$, $u_0^{(2)}$, $u_0^{(3)}$, $u_0^{(4)}$ and $u_0^{(5)}$ in the troubled cell Δ_0 is analogous to that for the $k=1$ case. The big stencil is shown in Fig. 2.

Step 2.4.1. We select the big stencil as $S=\{\Delta_0,\Delta_1,\Delta_2,\Delta_3,\Delta_{11},\Delta_{12},\Delta_{21},\Delta_{22},\Delta_{31},\Delta_{32}\}$. Then we construct polynomial $Q(x,y)$ to approximate u by requiring that it has the same cell average as $u^{(0)}$ on the target cell Δ_0 and matches the cell averages of $u^{(0)}$, $u^{(1)}$ or $u^{(2)}$ on the other triangles in the set $S\setminus\{\Delta_0\}$ in a least square sense.

Step 2.4.2. We can then construct quadratic polynomials $q_i(x,y),\ i=1,\ldots,9$, which satisfy the following conditions:

$$\frac{1}{|\Delta_\ell|}\int_{\Delta_\ell} q_i(x,y)\,dx\,dy = u_\ell^{(0)}, \tag{2.31}$$

$$\frac{1}{\int_{\Delta_{\ell_x}}(v_1^{(\ell_x)}(x,y))^2\,dx\,dy}\int_{\Delta_{\ell_x}} q_i(x,y)\,v_1^{(\ell_x)}(x,y)\,dx\,dy = u_{\ell_x}^{(1)}, \tag{2.32}$$

$$\frac{1}{\int_{\Delta_{\ell_y}}(v_2^{(\ell_y)}(x,y))^2\,dx\,dy}\int_{\Delta_{\ell_y}} q_i(x,y)\,v_2^{(\ell_y)}(x,y)\,dx\,dy = u_{\ell_y}^{(2)}. \tag{2.33}$$

For

$$\begin{aligned}
&i=1,\ \ell=0,1,11,12,3,32;\quad i=2,\ \ell=0,1,11,12,2,21;\quad i=3,\ \ell=0,2,21,22,1,12;\\
&i=4,\ \ell=0,2,21,22,3,31;\quad i=5,\ \ell=0,3,31,32,2,22;\quad i=6,\ \ell=0,3,31,32,1,11;\\
&i=7,\ \ell=0,1,11,12,\ \ell_x=1,\ \ell_y=1;\quad i=8,\ \ell=0,2,21,22,\ \ell_x=2,\ \ell_y=2;\\
&i=9,\ \ell=0,3,31,32,\ \ell_x=3,\ \ell_y=3.
\end{aligned}$$

The remaining steps are the same as those for the $k=1$ case. Finally, the moments of the reconstructed polynomial are given by:

$$u_0^{(l)}(t)=\frac{1}{\int_{\Delta_0}(v_l^{(0)}(x,y))^2\,dx\,dy}\sum_{i=1}^{9}\omega_i^{(l)}\int_{\Delta_0} q_i(x,y)\,v_l^{(0)}(x,y)\,dx\,dy,\quad l=1,2,3,4,5. \tag{2.34}$$

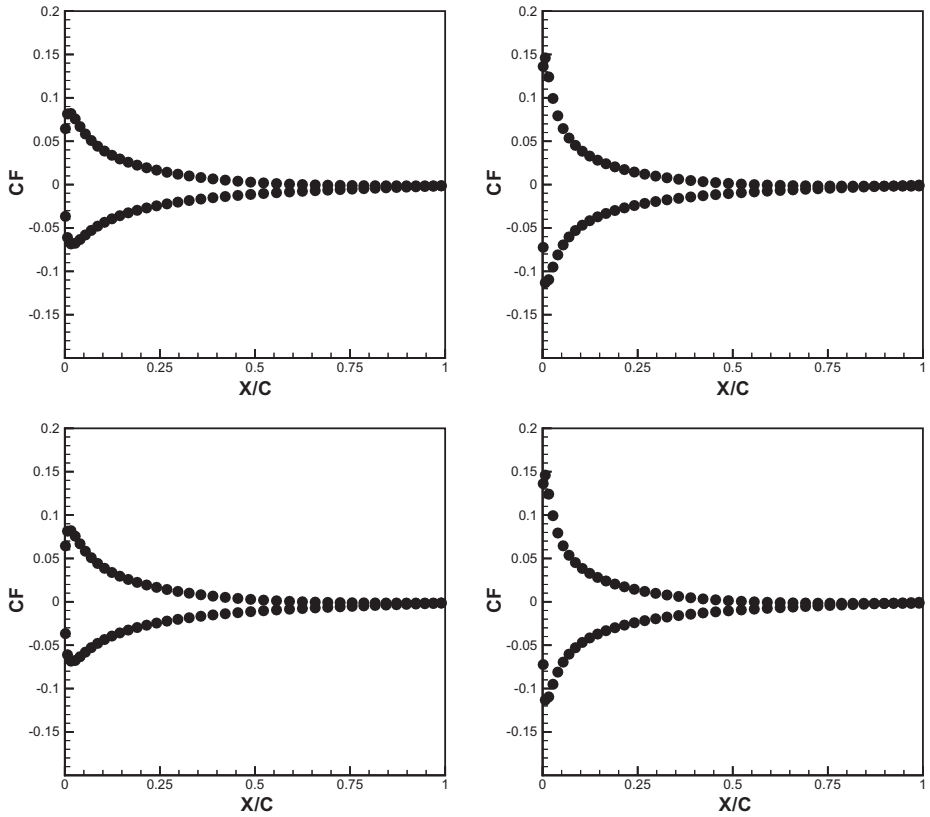

Fig. 19. NACA0012 airfoil. $M_\infty=0.5$, $Re_\infty=5000$ and $\alpha=2^\circ$. Skin friction coefficient distribution. Top: RKLDG with WENO limiter; bottom: RKLDG with HWENO limiter. Left: $k=1$; right: $k=2$.

3. Numerical results

In this section we provide numerical results to demonstrate the performance of the WENO and HWENO reconstructions limiters for the RKLDG methods on unstructured meshes described in Section 2.

We first test the accuracy of the schemes in two dimensional problems. And we assume unstructured mesh Γ_h, which has boundary triangle size h and then divided each triangle into four equally smaller triangles and denote associated unstructured mesh as $\Gamma_{\frac{h}{2}}$, which has boundary triangle size $\frac{h}{2}$. Then we use two different measurements of resolution and convergence:

(1) The problem has exact solution $u(x,y,t)$. The error at each point of the target cell is $e_i^h = u^h(x_i,y_i,t) - u(x_i,y_i,t)$. The L^1 and L^∞ convergence errors in the computational field are defined as: $\|e^h\|_{L^1} = \frac{1}{N}\sum_{i=1}^{N}|e_i^h|$ and $\|e^h\|_{L^\infty} = \max_{1\leqslant i\leqslant N}|e_i^h|$. And the numerical order of accuracy are given by:

$$r_{L^1} = \log_2\left(\frac{\|e^h\|_{L^1}}{\|e^{\frac{h}{2}}\|_{L^1}}\right), \tag{3.1}$$

$$r_{L^\infty} = \log_2\left(\frac{\|e^h\|_{L^\infty}}{\|e^{\frac{h}{2}}\|_{L^\infty}}\right). \tag{3.2}$$

We use this measurement in Example 3.1.

(2) The problem has not exact solution $u(x,y,t)$ and we now use the asymptotic convergence error estimation (see [25]) and define $er_i^h = u^h(x_i,y_i,t) - u^{\frac{h}{2}}(x_i,y_i,t)$. The L^1 and L^∞ convergence errors in the computational field are defined as: $\|er^h\|_{L^1} = \frac{1}{N}\sum_{i=1}^{N}|er_i^h|$ and $\|er^h\|_{L^\infty} = \max_{1\leqslant i\leqslant N}|er_i^h|$. And the numerical order of accuracy are given by:

$$rr_{L^1} = \log_2\left(\frac{\|er^h\|_{L^1}}{\|er^{\frac{h}{2}}\|_{L^1}}\right), \tag{3.3}$$

$$rr_{L^\infty} = \log_2\left(\frac{\|er^h\|_{L^\infty}}{\|er^{\frac{h}{2}}\|_{L^\infty}}\right). \tag{3.4}$$

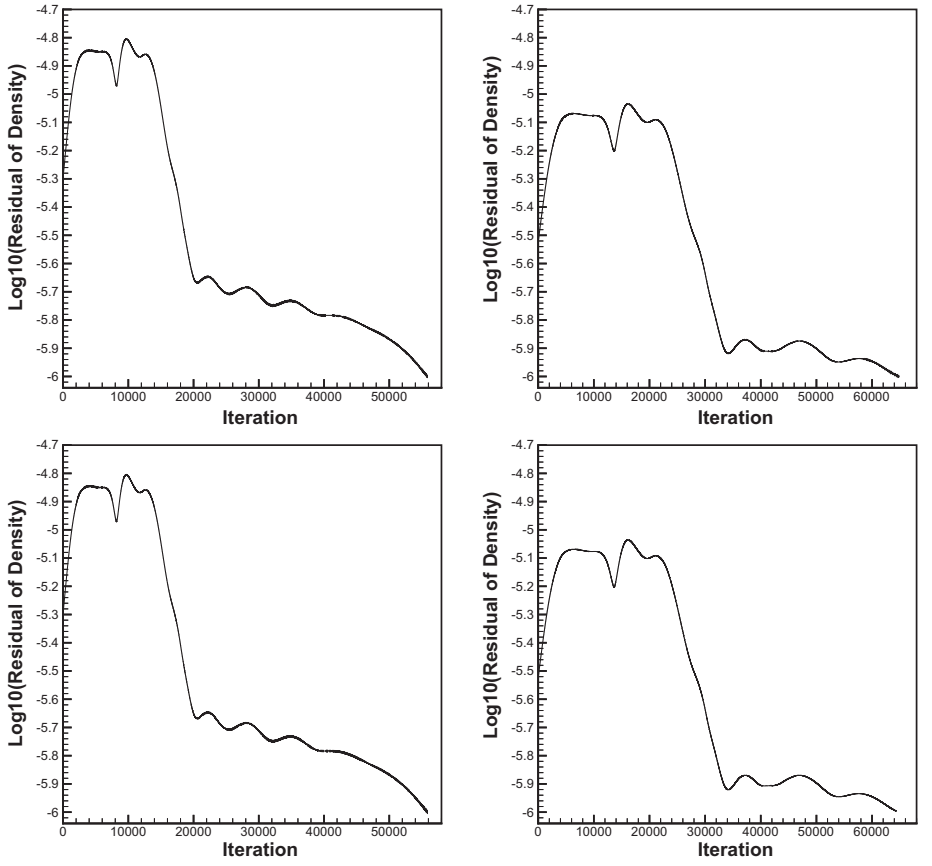

Fig. 20. NACA0012 airfoil. $M_\infty = 0.8$, $Re_\infty = 73$ and $\alpha = 10^\circ$. Reduction of density residual as a function of the number of iterations. Top: RKLDG with WENO limiter; bottom: RKLDG with HWENO limiter. Left: $k = 1$; right:$k = 2$.

We use this measurement in Example 3.2.

Example 3.1. We solve the following linear scalar convection diffusion equation in two dimensions:

$$u_t + u_x + u_y = \frac{2a}{\pi^2} u_{xx} + \frac{2a}{\pi^2} u_{yy} \tag{3.5}$$

with the initial condition $u(x,y,0) = \sin(0.5\pi(x+y))$ and periodic boundary conditions in both directions. The exact solution is $u(x,y,t) = e^{-at}\sin(0.5\pi(x+y-2t))$. We choose $a = 0.01$ and compute the solution up to $t = 1$. For this test case, the coarsest mesh we use is shown in Fig. 3. The errors and numerical orders of accuracy for the RKLDG method with the WENO and HWENO limiters comparing with the original RKLDG method without limiters are shown in Tables 1 and 2. In order to magnify the possible effect of the WENO and HWENO limiters on accuracy, we have deliberately chosen a small TVB constant $M = 0.01$ so that many cells are identified as "troubled cells". We can see that the WENO and HWENO limiters keep the designed order of accuracy, however the magnitude of the errors are larger than that of the original RKLDG method on the same mesh.

Example 3.2. We solve the 2D Navier–Stokes equations:

$$\begin{aligned}
&\frac{\partial}{\partial t}\begin{pmatrix}\rho\\ \rho u\\ \rho v\\ E\end{pmatrix} + \frac{\partial}{\partial x}\begin{pmatrix}\rho u\\ \rho u^2 + p\\ \rho uv\\ u(E+p)\end{pmatrix} + \frac{\partial}{\partial y}\begin{pmatrix}\rho v\\ \rho uv\\ \rho v^2 + p\\ v(E+p)\end{pmatrix} - \frac{\bar{\sigma}}{Re_\infty}\left(\frac{\partial}{\partial x}\begin{pmatrix}0\\ 2\mu u_x + \lambda\mu(u_x+v_y)\\ \mu(v_x+u_y)\\ u(2\mu u_x + \lambda\mu(u_x+v_y)) + v\mu(v_x+u_y) + \frac{\gamma\mu}{(\gamma-1)Pr}\frac{\partial\left(\frac{p}{\rho}\right)}{\partial x}\end{pmatrix}\right.\\
&\left. + \frac{\partial}{\partial y}\begin{pmatrix}0\\ \mu(v_x+u_y)\\ 2\mu v_y + \lambda\mu(u_x+v_y)\\ u\mu(v_x+u_y) + v(2\mu v_y + \lambda\mu(u_x+v_y)) + \frac{\gamma\mu}{(\gamma-1)Pr}\frac{\partial\left(\frac{p}{\rho}\right)}{\partial y}\end{pmatrix}\right) = 0
\end{aligned} \tag{3.6}$$

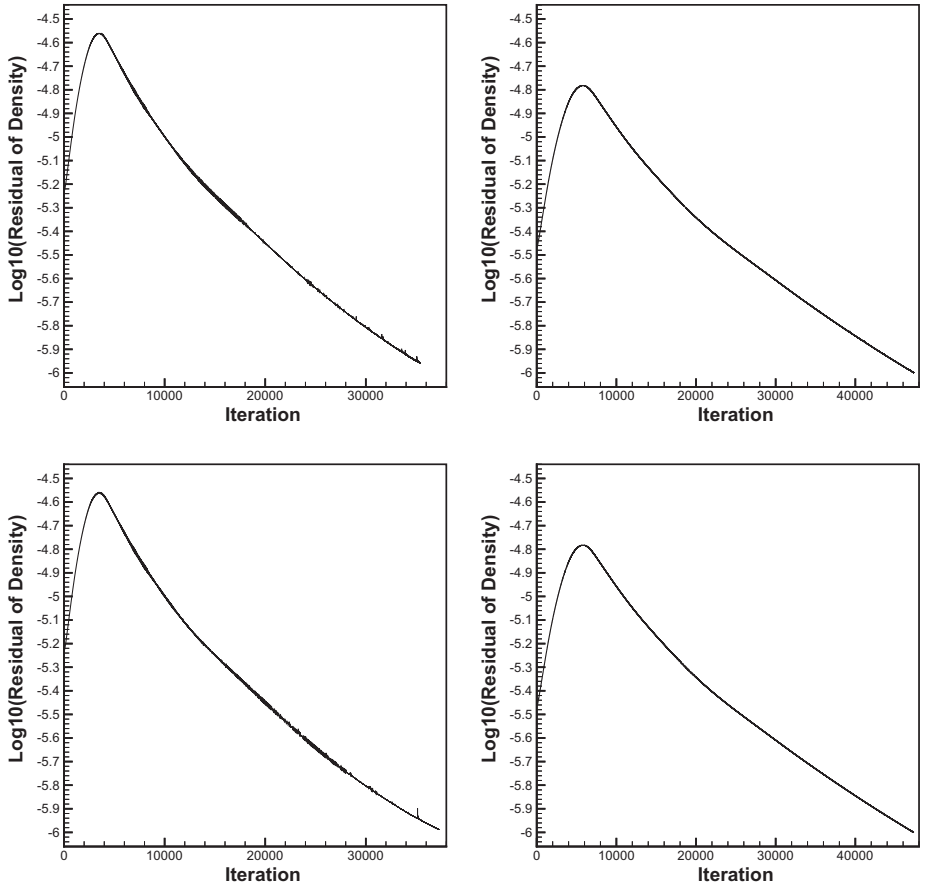

Fig. 21. NACA0012 airfoil. $M_\infty = 2$, $Re_\infty = 106$ and $\alpha = 10^\circ$. Reduction of density residual as a function of the number of iterations. Top: RKLDG with WENO limiter; bottom: RKLDG with HWENO limiter. Left: $k = 1$; right: $k = 2$.

in which ρ is the density, u is the x-direction velocity, v is the y-direction velocity, E is the total energy, $p = (\gamma - 1)\left(E - \frac{1}{2}\rho(u^2 + v^2)\right)$ is the pressure, $\gamma = 1.4,\ Re_\infty = 1000,\ \lambda = -2/3,\ \bar{\sigma} = 1,\ \mu = 1$ and $Pr = 0.72$. The initial conditions are: $\rho(x, y, 0) = 1 + 0.2\sin(\pi(x + y)),\ u(x, y, 0) = 0.5,\ v(x, y, 0) = 0.5,\ p(x, y, 0) = 1$. Periodic boundary conditions are applied in both directions. We compute the solution up to $t = 2$. For this test case, the coarsest mesh we use is shown in Fig. 4. The errors and numerical orders of accuracy of the density for the RKLDG method with the WENO and HWENO limiters comparing with the original RKLDG method without limiters are shown in Tables 3 and 4.

We now test the performance of the RKLDG method with the WENO and HWENO limiters for problems containing shocks. In general, the results are comparable when M is chosen adequately. The RKLDG method with the WENO and HWENO limiters produce much better results than those with the original *minmod* TVB limiter. From now on, we solve the Navier–Stokes equations (3.6) for the real simulations, set $\bar{\sigma} = \sqrt{\gamma}M_\infty$ and the coefficient of viscosity $\mu = \left(\frac{p}{\rho}\right)^{0.72}$.

Example 3.3. We first solve the laminar flow on the adiabatic flat plate characterized by a free-stream Mach number $M_\infty = 0.4$, $Re_\infty = 5000$ and $\alpha = 0^\circ$. The mesh used in the computation is shown in Fig. 5, 6000 elements obtained from the triangulation of a structured meshes. The size of the elements adjacent to the wall in the x-direction equals $\Delta x/L = 0.0125$, in the y-direction the minimum $\Delta y/L = 0.0001$. In Tables 5 and 6 we document the percentage of cells declared to be "troubled cells" for different orders of accuracy and different TVB constant M in the *minmod* limiter to identify troubled cells. The velocities normally to the plate are shown in Fig. 6.

Example 3.4. We consider transonic flow past a single NACA0012 airfoil configuration with three different initial conditions. Case 1: $M_\infty = 0.8,\ Re_\infty = 73$ and $\alpha = 10^\circ$; case 2: $M_\infty = 2,\ Re_\infty = 106$ and $\alpha = 10^\circ$; case 3: $M_\infty = 0.85,\ Re_\infty = 2000$ and $\alpha = 0^\circ$; case 4: $M_\infty = 0.5,\ Re_\infty = 5000$ and $\alpha = 2^\circ$. The computational domain is $[-50, 50] \times [-50, 50]$. The mesh used in the computation is shown in Fig. 7, consisting of 12,800 elements with the maximum diameter of the circumcircle being 34.976 and the minimum diameter being 0.011 near the airfoil. The different order RKLDG schemes with the WENO and HWENO limiters and the TVB constant $M = 1,\ M = 10$ and $M = 100$ are used in the numerical experiments. In Table 7, we document the percentage of cells declared to be "troubled cells" for different orders of accuracy and different TVB constant M in the

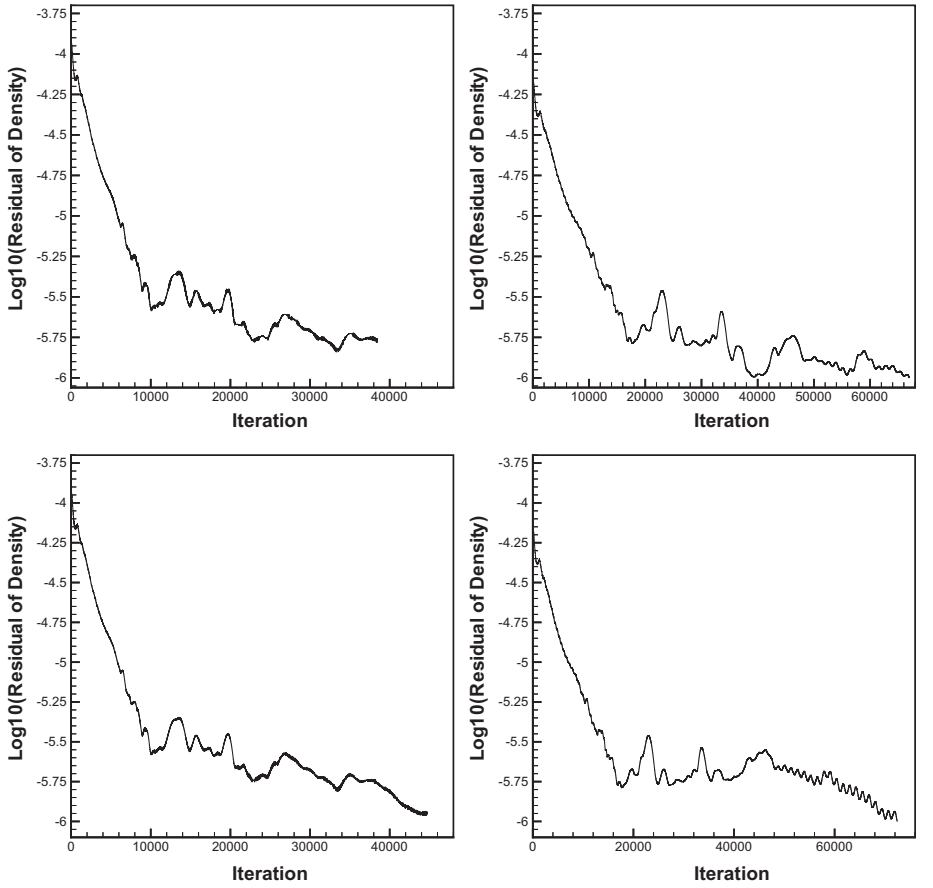

Fig. 22. NACA0012 airfoil. $M_\infty = 0.85,\ Re_\infty = 2000$ and $\alpha = 0^\circ$. Reduction of density residual as a function of the number of iterations. Top: RKLDG with WENO limiter; bottom: RKLDG with HWENO limiter. Left: $k = 1$; right: $k = 2$.

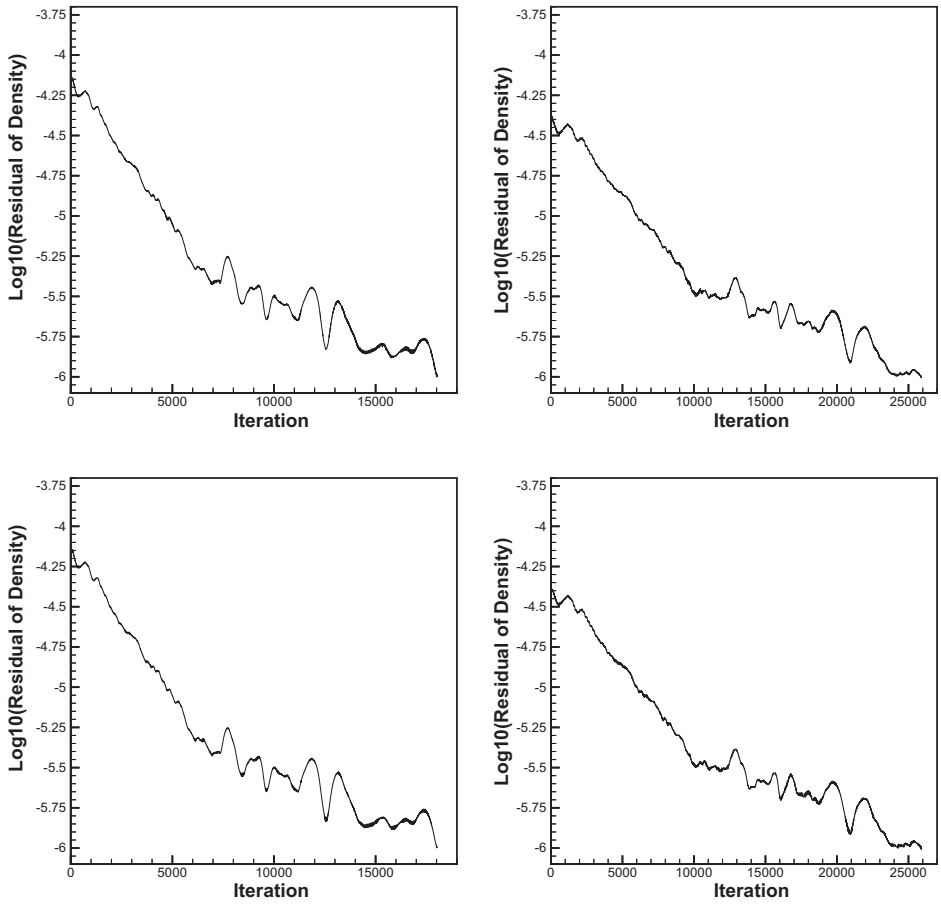

Fig. 23. NACA0012 airfoil. $M_\infty = 0.5$, $Re_\infty = 5000$ and $\alpha = 2^\circ$. Reduction of density residual as a function of the number of iterations. Top: RKLDG with WENO limiter; bottom: RKLDG with HWENO limiter. Left: $k = 1$; right: $k = 2$.

minmod limiter to identify troubled cells. We can see that only a small percentage of cells are declared as "troubled cells" for large M. In Table 8, we give the lift, drag and moment of force coefficients subject to the WENO and HWENO limiters. Mach number, pressure distribution and skin friction coefficient distribution are shown in Figs. 8–18, respectively, and only figures for TVB constant $M = 100$ are shown to save space. We can see that the third order schemes have better resolutions than the second order ones. Finally, the reduction of density residual as a function of the number of iterations are shown in Figs. 19–23. For Test Case 1 and 2, we plot the pressure distribution and skin friction coefficient distribution by the second and the third order RKLDG methods with WENO and HWENO limiter against numerical solution of [1] with the forth order ($k = 3$). We can see that the results of RKLDG methods with WENO and HWENO limiter and method in [1] are similar.

4. Concluding remarks

We have developed limiters for the RKLDG methods solving compressible Navier–Stokes equations using finite volume high order WENO and HWENO reconstructions on unstructured meshes. The ideas are to first identify troubled cells subject to the WENO and HWENO limitings, using a TVB *minmod*-type limiter, then reconstruct the algebraic polynomial solution inside the troubled cells by the WENO and HWENO reconstructions using the cell averages or derivative cell averages of neighboring cells, while maintaining the original cell averages of the troubled cells. Numerical results are provided to show that the methods are stable, accurate, and robust in maintaining accuracy.

Acknowledgment

The research was partially supported by NSFC Grant 10931004, 10671091, 10811120283, 10871093 and the European project ADIGMA on the development of innovative solution algorithms for aerodynamic simulations. Additional support

was provided by USA NSF DMS-0820348 while J. Qiu was in residence at Department of Mathematical Sciences, Rensselaer Polytechnic Institute.

References

[1] F. Bassi, S. Rebay, A high-order accurate discontinuous finite element method for the numerical solution of the compressible Navier–Stokes equations, Journal of Computational Physics 131 (1997) 267–279.
[2] R. Biswas, K.D. Devine, J. Flaherty, Parallel, adaptive finite element methods for conservation laws, Applied Numerical Mathematics 14 (1994) 255–283.
[3] A. Burbeau, P. Sagaut, C.H. Bruneau, A problem-independent limiter for high-order Runge–Kutta discontinuous Galerkin methods, Journal of Computational Physics 169 (2001) 111–150.
[4] B. Cockburn, S. Hou, C.-W. Shu, The Runge–Kutta local projection discontinuous Galerkin finite element method for conservation laws IV: the multidimensional case, Mathematics of Computation 54 (1990) 545–581.
[5] B. Cockburn, S.-Y. Lin, C.-W. Shu, TVB Runge–Kutta local projection discontinuous Galerkin finite element method for conservation laws III: one dimensional systems, Journal of Computational Physics 84 (1989) 90–113.
[6] B. Cockburn, C.-W. Shu, TVB Runge–Kutta local projection discontinuous Galerkin finite element method for conservation laws II: general framework, Mathematics of Computation 52 (1989) 411–435.
[7] B. Cockburn, C.-W. Shu, The Runge–Kutta local projection P1-discontinuous Galerkin finite element method for scalar conservation laws, Mathematical Modelling and Numerical Analysis (M^2AN) 25 (1991) 337–361.
[8] B. Cockburn, C.-W. Shu, The Runge–Kutta discontinuous Galerkin method for conservation laws V: multidimensional systems, Journal of Computational Physics 141 (1998) 199–224.
[9] B. Cockburn, C.-W. Shu, The local discontinuous Galerkin method for time-dependent convection-diffusion systems, SIAM Journal on Numerical Analysis 35 (6) (1998) 2440–2463.
[10] B. Cockburn, C.-W. Shu, Runge–Kutta discontinuous Galerkin method for convection-dominated problems, Journal of Scientific Computing 16 (2001) 173–261.
[11] O. Friedrichs, Weighted essentially non-oscillatory schemes for the interpolation of mean values on unstructured grids, Journal of Computational Physics 144 (1998) 194–212.
[12] G. Gassner, F. Löcher, C.-D. Munz, A contribution to the construction of diffusion fluxes for finite volume and discontinuous Galerkin schemes, Journal of Computational Physics 224 (2007) 1049–1063.
[13] C. Hu, C.-W. Shu, Weighted essentially non-oscillatory schemes on triangular meshes, Journal of Computational Physics 150 (1999) 97–127.
[14] G. Jiang, C.-W. Shu, Efficient implementation of weighted ENO schemes, Journal of Computational Physics 126 (1996) 202–228.
[15] X. Liu, S. Osher, T. Chan, Weighted essentially non-oscillatory schemes, Journal of Computational Physics 115 (1994) 200–212.
[16] I. Lomtev, G.E. Karniadakis, A discontinuous Galerkin method for the Navier–Stokes equations, International Journal of Numerical Methods Fluids 29 (1999) 587–603.
[17] H. Luo, J.D. Baum, R. Lohner, A Hermite WENO-based limiter for discontinuous Galerkin method on unstructured grids, Journal of Computational Physics 225 (2007) 686–713.
[18] J. Qiu, C.-W. Shu, Hermite WENO schemes and their application as limiters for Runge–Kutta discontinuous Galerkin method: one dimensional case, Journal of Computational Physics 193 (2004) 115–135.
[19] J. Qiu, C.-W. Shu, Runge–Kutta discontinuous Galerkin method using WENO limiters, SIAM Journal on Scientific Computing 26 (2005) 907–929.
[20] J. Qiu, C.-W. Shu, Hermite WENO schemes and their application as limiters for Runge–Kutta discontinuous Galerkin method II: two dimensional case, Computers and Fluids 34 (2005) 642–663.
[21] W.H. Reed, T.R. Hill, Triangular Mesh Methods for Neutron Transport Equation, Tech. Report LA-UR-73-479, Los Alamos Scientific Laboratory, 1973.
[22] J. Shi, C. Hu, C.-W. Shu, A technique of treating negative weights in WENO schemes, Journal of Computational Physics 175 (2002) 108–127.
[23] C.-W. Shu, TVB uniformly high-order schemes for conservation laws, Mathematics of Computation 49 (1987) 105–121.
[24] C.-W. Shu, S. Osher, Efficient implementation of essentially non-oscillatory shock-capturing schemes, Journal of Computational Physics 77 (1988) 439–471.
[25] Y.T. Zhang, J. Shi, C.-W. Shu, Y. Zhou, Numerical viscosity and resolution of high-order weighted essentially nonoscillatory schemes for compressible flows with high Reynolds numbers, Physical Review 68 (2003) 046709.
[26] J. Zhu, J. Qiu, Hermite WENO schemes and their application as limiters for Runge–Kutta discontinuous Galerkin method III: unstructured meshes, Journal of Scientific Computing 39 (2009) 293–321.
[27] J. Zhu, J. Qiu, C.-W. Shu, M. Dumbser, Runge–Kutta discontinuous Galerkin method using WENO limiters II: unstructured meshes, Journal of Computational Physics 227 (2008) 4330–4353.